UNIVERSITÀ DEGLI STUDI DI PADOVA

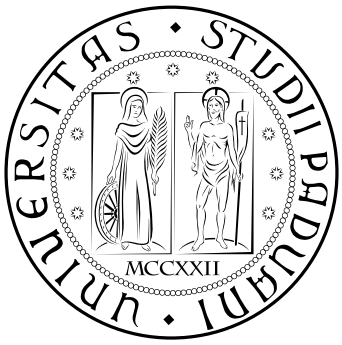

FACOLTÀ
DI SCIENZE MM. FF. NN.

Dip. di Fisica e Astronomia "Galileo Galilei"

UNIVERSITÄT ZÜRICH

MATHEMATISCH-NATURWISSENSCHAFTLICHE
FAKULTÄT

Physik-Institut

Scuola di Dottorato di Ricerca in Fisica
Ciclo XXVI

Electromagnetic dipole moments of fermions

Supervisor: Dr. Massimo Passera

Supervisor: Prof. Dr. Thomas Gehrmann

Direttore della Scuola:
Ch.mo Prof. Andrea Vitturi

Ph.D. Candidate: Matteo Fael

"The more important fundamental laws and facts of physical science have all been discovered, and these are so firmly established that the possibility of their ever being supplanted in consequence of new discoveries is exceedingly remote ...
... our future discoveries must be looked for in the sixth place of decimals."

A. A. Michelson, in "Light Waves and Their Uses",
University of Chicago Press (1903), pp 23-25

Abstract

The electric (EDM) and magnetic ($g-2$) dipole moments are static properties sensitive to quantum corrections induced by the virtual particles that populate the vacuum. Indeed, they are well suited to test the Standard Model of Elementary of particle physics and to unveil unknown New Physics (NP) hidden at high energy. The electron and muon $g-2$ have been measured with the wonderful precision of 0.24 ppb and 0.54 ppm, respectively, and thus they represent one of the strongest confirmation of the SM and greatest achievement in Quantum Field Theory.

Nonetheless the SM deficiencies, the explanation of dark matter and dark energy, cosmological inflaton, neutrino oscillations and masses, the strong CP problem and the origin of matter-antimatter asymmetry, call for new physics beyond the SM. Since NP contribution to the dipole moments of a fermion f is expected to be proportional to m_f^2, dipole moments of heavy fermions, such as the top quark or the tau lepton, are much more sensitive to NP effects than the electron or muon ones. However the very short lifetime of these unstables particle makes it impossible to directly measure their electromagnetic properties. Therefore, indirect information must be obtain by precisely measuring cross sections and decay rates in processes involving the emission of a real photon by the heavy fermion.

In this thesis, we investigate the possibility to measure the anomalous magnetic moment and the electric dipole moment of the top quark at the LHC and tau lepton at future high luminosity B-factories.

Contents

To Elisa

Introduction

The electric (EDM) and magnetic ($g-2$) dipole moments are static properties sensitive to quantum corrections induced by the virtual particles that populate the vacuum. Indeed, they are well suited to test the Standard Model of Elementary of particle physics and to unveil unknown New Physics (NP) hidden at high energy. The electron and muon $g-2$ have been measured with the wonderful precision of 0.24 ppb[1] and 0.54 ppm[2], respectively, and thus they represent one of the greatest achievement in Quantum Field Theory and strongest confirmation of the SM.

Nonetheless the SM deficiencies, the explanation of dark matter and dark energy, cosmological inflaton, neutrino oscillations and masses, the strong CP problem and the origin of matter-antimatter asymmetry, call for new physics beyond the SM. In a large class of theories beyond the SM [3–5], new contributions to the $g-2$ of a fermion f are expected to modify the Standard Model (SM) prediction by a term proportional to m_f^2. So, for example, from a pure theoretical point of view the $g-2$ of the tau is much more sensitive to New Physics (NP) effects than the muon and electron ones. Also, in view of its large mass, the top quark is even better suited to unveil deviations from the SM and to probe the dynamics that breaks the electroweak gauge symmetry. Furthermore, compared to the other quarks, the top features are not spoiled by low-energy QCD effects since the top quark decays before hadronizing.

EDM interactions violate parity and time reversal, so that if CPT is a good symmetry, T violation implies CP violation and vice versa. The SM values for lepton and quark fundamental EDMs are astonishingly small, too tiny to be seen by the projected future experiments. Hence, the observation of a non-vanishing fundamental EDM would be bright evidence for a CP-violating NP effect [6, 7].

However a very short lifetime poses many difficulties for the experimental determination of dipole moments whose bounds must therefore be obtained in an indirect way through precise measurements of cross sections and decay widths. In fact, while indirect limits on anomalous electromagnetic couplings from electroweak precision data or flavor physics

observables turn out to be very constraining for bottom quarks [8–10], only loose bounds can be obtained in the case of top quarks [11, 12]. Nonetheless, several studies have established photon radiation in top pair production at hadron colliders as potential probe of anomalous coupling effects [13], which could be improved upon only at a future high-energy electron-positron collider [14].

In this thesis we propose single-top-plus-photon production as a tool to investigate the $t\gamma$ coupling at the LHC.Indeed, with the cross sections for top pair production and single-top production being of comparable magnitude at this hadron collider, it appeared worthwhile to extend the $t\bar{t}\gamma$ production analysis in [13] to photon radiation in single top quark production. In this work we analyze in detail signal and background processes contributing to single-top-plus-photon production and we quantify the numerical magnitude of the top dipole moments that can be detected in the upcoming 14 TeV runs at the LHC. In the end, we give compelling reasons to analyze single-top-plus-gamma at the LHC by demonstrating that the bounds that can be obtained from single-top-plus-photon production are very much comparable in magnitude to those that can be obtained from $t\bar{t}\gamma$ final states. These channels are completely independent from each other and therefore can be further combined. In particular, we will show that existing bounds may be improved upon by up to one order of magnitude.

High luminosity B- and τ/charm-factories offer new opportunities in tau precision physics thanks to their high statistics and energy resolution. In particular, concerning the study of dipole moments at B-factories, in Ref. [15] it has been proposed to search for the tau anomalous magnetic moment form factor in tau pair production at the Υ resonances. However the beam energy spread at Belle and future Belle-II makes very difficult to resolve these narrow resonances.

For this reason we suggest in this thesis an alternative measurement of the tau anomalous magnetic moment via leptonic radiative decays $\tau \to l\nu_\tau\bar{\nu}_l\gamma$ with a precision of $\mathcal{O}(10^{-3})$, which is the magnitude of the leading SM contribution. In fact the very short lifetime of the tau has so far prevented the direct determination its $g-2$ by measuring its spin precession as in the muon experiment, and the present resolution on its anomalous magnetic moment [16] is more than an order of magnitude larger than its SM prediction [17].

Without any QCD low-energy approximation, the proposed study of leptonic radiative decays offer the clean theoretical environment required by the desired experimental precision. To provide the theoretical framework for such measurements at $\mathcal{O}(10^{-3})$, we computed the polarized differential decay rate at NLO in the SM, including also W-boson propagator effects and possible non-vanishing $g-2$ and EDM contributions. As shown long ago in Ref. [18], to leading order in G_F but to all orders in α, the radiative corrections to muon

decay are finite in the Fermi V-A theory after mass and charge renormalization. Since this special feature holds also for taus decaying into leptons, we computed all NLO corrections to radiative leptonic decays in the Fermi theory, including full mass dependence.

In a dedicated feasybility study it has been analyzed the whole data sample collected at Belle and planned in Belle II experiment in order to establish which are the future achievable sensitivities to the tau dipole moments in radiative leptonic decays. We will show that the measurement of tau anomalous magnetic moment at Belle II can be already competitive with the current bound from DELPHI experiment [16]. While the expected sensitivity to the tau EDM is still worse than the most precise measurement done at Belle [19].

Chapter 1

Radiative decays of tau lepton

1.1 General $ff\gamma$ coupling

The most general Lorentz-invariant vertex function describing the interaction of two on-shell fermions and a photon can be written in the form

$$\Gamma_\mu(q^2) = -ie\left\{\gamma_\mu\left[F_{1V}(q^2) + F_{1A}(q^2)\gamma_5\right] + \frac{\sigma_{\mu\nu}}{2m_f}q^\nu\left[iF_{2V}(q^2) + F_{2A}(q^2)\gamma_5\right]\right\}, \tag{1.1}$$

where e is the proton charge, m_f the mass of the fermion, $\sigma_{\mu\nu} = i/2\left[\gamma_\mu, \gamma_\nu\right]$ and q is the four-momentum of the off-shell photon. The functions $F_i(q^2)$ are called the form factors and in the limit $q^2 \to 0$ they are physical and related to the static quantities

$$\begin{aligned} F_{1V}(0) &= Q_f, \\ F_{2V}(0) &= a_f\, Q_f, \\ F_{2A}(0) &= d_f\, \frac{2m_f}{e}, \end{aligned} \tag{1.2}$$

where Q_f is the charge of the fermion, a_f and d_f are, respectively, the anomalous magnetic moment and the electric dipole moment. The electric dipole contribution $F_{2A}(q^2)$ violates T and P invariance and therefore CP-invariance (if CPT is a good symmetry of nature). Indeed, EDM vanishes in any CP-conserving theory.

It is illustrative also to combine the two (real) dipole moments, a_f and d_f into a single complex dipole moment [20]:

$$c_f = a_f\frac{Q_f e}{2m_f} - id_f. \tag{1.3}$$

Thanks to this definition, in the limit $q^2 \to 0$ the dipole moments interactions in Eq. (1.1) can be recast as

$$[c_R\, \sigma_{\mu\nu} P_R + c_L\, \sigma_{\mu\nu} P_L]\, q^\nu, \tag{1.4}$$

where P_R and P_L are, respectively, the right and left-handed chiral spinor projectors. If we renounce CPT invariance, c_R and c_L are general and the dipole moments can acquire any complex values Here we anticipate that in the feasibility study of tau dipole moments we chose, for completeness, a_τ and d_τ to be complex number. However, if we require the interaction of (1.4) to be hermitian, then $c_f \equiv c_L = c_R^*$, i.e. a_f and d_f must to be real parameters.

We noted that in general direct production processes of the fermion f are not suited to disentangle the contributions from the CP-conserving magnetic dipole moment a_f and the CP-violating electric dipole moment d_f. As a matter of fact, production amplitudes will usually probe the modulus of the complex dipole moment, i.e. the combination

$$|c_f| = \sqrt{\left(a_f \frac{Q_f e}{2m_f}\right)^2 + d_f^2}, \tag{1.5}$$

whereas they are almost insensitive to the phase,

$$\tan(\varphi_f) = \frac{d_f}{a_f}\frac{2m_f}{Q_f e}, \tag{1.6}$$

that can be regarded also as a measure of CP violation. The phases, φ_f, defined above are all expected to be very small (except possibly in the case of a Dirac neutrino where the anomalous magnetic moment and electric dipole moment are both tiny). As such, they are not very useful except as a reminder that CP violation is generally a very small effect.

1.2 The SM prediction of a_τ

In this section we briefly recall the SM prediction for the tau anomalous magnetic moment, a_τ, that is given by the sum of QED, electroweak (EW) and hadronic (HAD) terms (for a more exhaustive analysis we refer the reader to refs. [17, 21]). All reported results were derived using the CODATA [22] recommended mass ratios,

$$m_\tau/m_e = 3477.48\ (57), \tag{1.7}$$

$$m_\tau/m_\mu = 16.8183\ (27). \tag{1.8}$$

The value for m_τ adopted by CODATA in ref. [22], $m_\tau = 1776.99\,(29)$ MeV, is based on the PDG 2002 results [23].

1.2.1 QED contribution

The QED part, $a_\tau^{\rm QED}$, arises from the subset of SM diagrams containing only leptons and photons. This dimensionless quantity can be cast in the general form [24]:

$$a_\tau^{\rm QED} = A_1 + A_2\left(\frac{m_\tau}{m_e}\right) + A_2\left(\frac{m_\tau}{m_\mu}\right) + A_3\left(\frac{m_\tau}{m_e}, \frac{m_\tau}{m_\mu}\right), \tag{1.9}$$

where m_e, m_μ, and m_τ are the electron, muon, and τ mass.

The term A_1, arising from diagrams containing only photons and τ, is mass and flavour independent. In contrast the terms A_2 and A_3 are functions of the indicated mass ratios and are generated by graphs including also electrons and muons. Each function A_i can be expanded as power series in α/π and computed order by order:

$$A_i = A_i^{(2)}\left(\frac{\alpha}{\pi}\right) + A_i^{(4)}\left(\frac{\alpha}{\pi}\right)^2 + A_i^{(6)}\left(\frac{\alpha}{\pi}\right)^3 + \cdots . \tag{1.10}$$

Only one diagram is involved in the evaluation of the one-loop contribution.

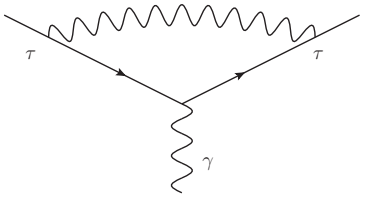

It provides the famous mass independent result of Schwinger [25]

$$a_1^{\rm QED} = \frac{\alpha}{2\pi}, \tag{1.11}$$

and so $A_1^{(2)} = 1/2$.

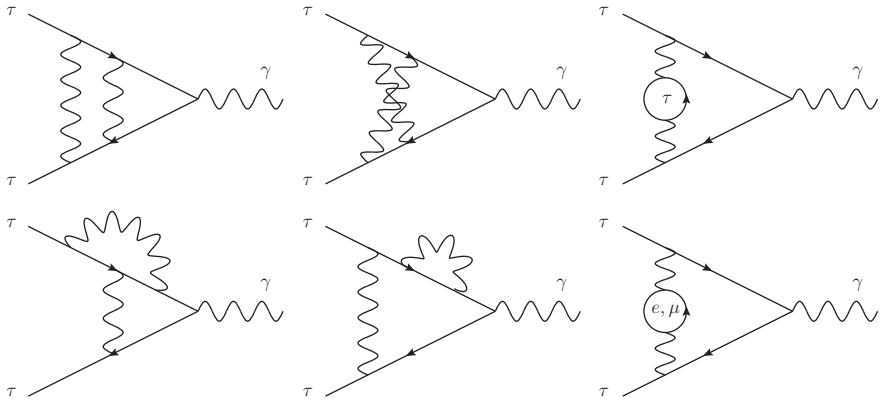

FIGURE 1.1: The QED two-loop corrections to a_τ.

At two-loop, see Fig. 1.1, seven diagrams contribute to the second order term $A_1^{(4)}$ and one to $A_2^{(4)}$. The mass independent term has the analytical expression [26]

$$A_2^{(2)} = \frac{197}{144} + \frac{\pi^2}{12} + \frac{3}{4}\zeta(3) - \frac{\pi^2}{2}\ln 2, \tag{1.12}$$

where $\zeta(z)$ is the Riemann zeta function. The coefficient of the two-loop mass-dependent contribution $A_2^{(4)}(1/x)$, with $x = m_e/m_\tau$ or m_μ/m_τ, is generated by the diagram with a vacuum polarization subgraph containing the virtual lepton e or μ. The exact result has the analytic compact form [27, 28]

$$\begin{aligned} A_2^{(4)}\left(\frac{1}{x}\right) = &-\frac{25}{36} - \frac{\ln x}{3} + x^2(4 + 3\ln x) + \frac{x}{2}(1 - 5x^2) \\ &\times \left[\frac{\pi^2}{2} - \ln x \ln\left(\frac{1-x}{1+x}\right) - \mathrm{Li}_2(x) + \mathrm{Li}_2(-x)\right] \\ &+ x^4\left[\frac{\pi^2}{3} - 2\ln x \ln\left(\frac{1}{x} - x\right) - \mathrm{Li}_2(x^2)\right], \end{aligned} \tag{1.13}$$

where $\mathrm{Li}_2(z)$ is the dilogarithm defined as

$$\mathrm{Li}_2(z) = -\int_0^z \frac{\ln(1-t)}{t} dt. \tag{1.14}$$

The numerical values for the fourth order A_i coefficients are reported in Tab. 1.1. Note that the errors are only due to the uncertainties of the mass ratios. The total fourth order contribution is

$$A_1^{(4)} + A_2^{(4)}(m_\tau/m_e) + A_2^{(4)}(m_\tau/m_\mu) = 2.057\,457\,(93). \tag{1.15}$$

term	value
$A_1^{(4)}$	$-\ 0.328\,478\ \cdots$
$A_2^{(4)}(m_\tau/m_e)$	$\ \ 2.024\,284\,(55)$
$A_2^{(4)}(m_\tau/m_\mu)$	$\ \ 0.361\,652\,(38)$

TABLE 1.1: numerical values for the fourth order A_i coefficients [29]

More than one hundred diagrams contribute to the QED three-loop correction. The coefficient $A_1^{(6)}$ arises from 72 diagrams. Its exact expression is [30]

$$\begin{aligned} A_1^{(6)} = &\frac{83}{72}\pi^2\zeta(3) - \frac{215}{24}\zeta(5) - \frac{239}{2160}\pi^4 + \frac{28259}{5184} + \frac{139}{18}\zeta(3) \\ &- \frac{298}{9}\pi^2\ln 2 + \frac{17101}{810}\pi^2 + \frac{100}{3}\left[\mathrm{Li}_4\left(\frac{1}{2}\right) + \frac{1}{24}(\ln^2 2 - \pi^2)\ln^2 2\right]. \end{aligned} \tag{1.16}$$

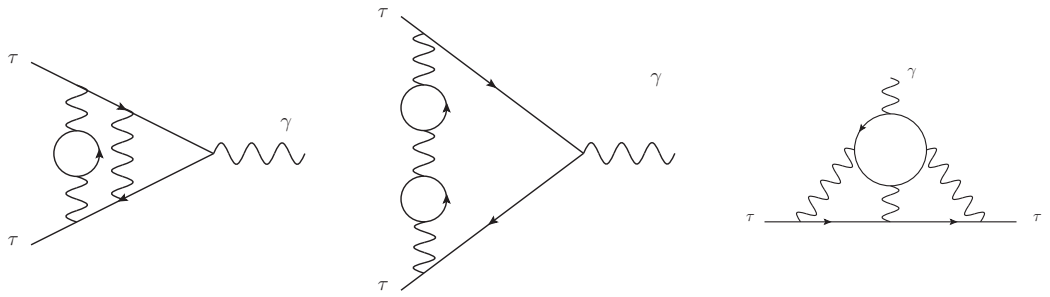

(A) Vacuum polarization type

(B) Double vacuum polarization

(C) Light-by-light

FIGURE 1.2: Some QED three loop diagrams contributions to a_τ.

The coefficients $A_2^{(6)}(m_\tau/m_i)$, $i = \mu, e$, can be further split into two parts: the first one $A_2^{(6)}(m_\tau/m_i, vac)$ receives contributions from 36 diagrams containing either electron or muon vacuum polarization loops (see for example Fig. 1.2a), whereas the second one, $A_2^{(6)}(m_\tau/m_i, lbl)$, is due to 12 light-by-light scattering diagrams with either electron and muon loops (see Fig. 1.2b). The coefficient $A_3^{(6)}$ arises from diagrams with two-loop vacuum polarization subgraphs. The values of three-loop coefficients are reported in Tab. 1.2. The errors are due to the mass ratio uncertainties (see the beginning of this section). Adding these results one finds:

$$\sum_i A_i^{(6)} = 57.9315\,(27). \tag{1.17}$$

term	value
$A_1^{(6)}$	$1.181\,241\,456\,\cdots$
$A_2^{(6)}(m_\tau/m_e)$	46.392 1 (15)
$A_2^{(6)}(m_\tau/m_\mu)$	7.010 21 (76)
$A_3^{(6)}(m_\tau/m_e,\ m_\tau/m_\mu)$	3.347 97 (41)

TABLE 1.2: numerical values for the sixth order A_i coefficients [29]

QED terms of order higher than three are not known. So the total QED contribution to a_τ is [29]

$$a_\tau^{\rm QED} = 117\,324\,(2)\ \cdot\ 10^{-8} \tag{1.18}$$

The error $\delta a_\tau^{\rm QED}$ is the uncertainty $\delta C_\tau^{(8)}(\alpha/\pi)^4 \sim \pi^2 \ln^2(m_\tau/m_e)(\alpha/\pi)^4 \sim 2 \cdot 10^{-8}$ that the author in Ref. [29] assigned to $a_\tau^{\rm QED}$ for the uncalculated four-loop contributions. Compared to this one, the errors due to the uncertainties of the $O(\alpha^2)$ and $O(\alpha^3)$ terms are negligible.

1.2.2 Electroweak contribution

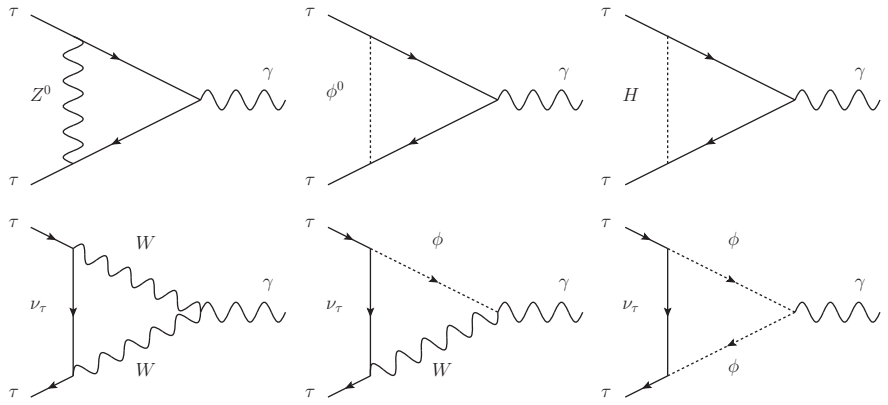

FIGURE 1.3: The one-loop electroweak contributions to a_τ. The diagram with a W and a Goldstone boson ϕ must be counted twice.

With respect to the QED one-loop term, the electroweak correction to a_τ is suppressed by the ratio $(m_\tau/M_W)^2 \approx 4.8 \cdot 10^{-4}$, where $M_W = 80.399(23)$ GeV is the mass of W boson [31]. The EW contribution is therefore of the same order of magnitude as the three-loop QED one. The one-loop diagrams involved are shown in Fig. 1.3. The analytic expression for the one-loop EW contribution to a_τ reads [32–36]

$$a_\tau^{\mathrm{EW}}(\text{one-loop}) = \frac{5G_F m_\tau^2}{24\sqrt{2}\pi^2}\left[1 + \frac{1}{5}(1 - 4\sin^2\theta_W)^2 + O\left(\frac{m_\tau^2}{M_{Z,W,H}^2}\right)\right], \tag{1.19}$$

where $G_F = 1.6637(1)\cdot 10^{-5}\mathrm{GeV}^{-2}$ is the Fermi coupling constant [31], M_Z, M_W, M_H are the masses of the Z, W and Higgs bosons, and $\sin^2\theta_W(M_Z) = 0.231\,22(15)$ is the Weinberg angle [31]. From the last equation we get [17]

$$a_\tau^{\mathrm{EW}}(\text{one-loop}) = 55.2\,(1)\cdot 10^{-8}. \tag{1.20}$$

The two-loop correction to a_τ^{EW} involves 1678 diagrams [37, 38]. Naively one would expect the two-loop EW terms to be of order $(\alpha/\pi)\cdot a_\tau^{\mathrm{EW}}$ and thus negligible, on the contrary they contribute quite substantially because of the appearance of terms enhanced by a factor of $\log(M_{W,Z}/m_f)$, where m_f is a fermion mass scale much smaller than M_W. The two-loop EW contribution is [17, 38]

$$a_\tau^{\mathrm{EW}}(\text{two-loop}) = -7.74\cdot 10^{-8}, \tag{1.21}$$

a 14% reduction of the one-loop result. The three-loop EW corrections to a_τ were determined to be extremely small via renormalization-group analysis [39]. The total EW

part is [17]

$$a_\tau^{\mathrm{EW}} = 47.4\,(5)\cdot 10^{-8}. \tag{1.22}$$

1.2.3 The Hadronic Contribution

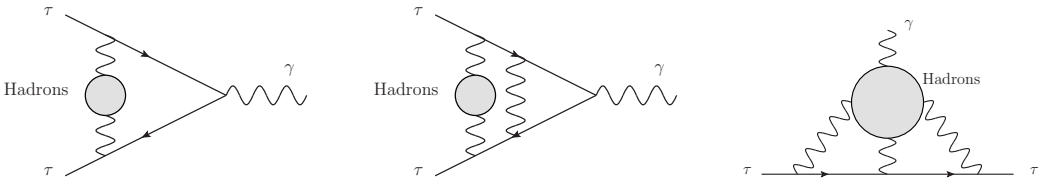

(A) Leading order correction (B) A higher order correction (C) Light-by-light

FIGURE 1.4: Examples of hadronic contributions to a_τ.

Unlike the QED part, the contribution from quantum fluctuations involving hadrons cannot be computed from theory alone, because most of the hadronic physics occurs in the low-energy non-perturbative QCD regime. At the leading-order (α^2) the corresponding Feynman diagram is shown in fig. 1.4, which involves one hadronic insertion. By virtue of the analyticity structure of the vacuum polarization correlator, the hadronic contribution to the magnetic anomaly can be calculated via the dispersion integral [40–43]:

$$a_\tau^{\mathrm{HLO}} = \frac{m_\tau^2}{12\pi^3}\int_{4m_\pi^2}^{\infty} ds \frac{\sigma^{(0)}(e^+e^-\to \text{hadrons})K_\tau(s)}{s}, \tag{1.23}$$

where $\sigma^{(0)}(e^+e^-\to \text{hadrons})$ is the total hadronic cross section of the e^+e^- annihilation in the Born approximation, and $K_\tau(s)$ is a bounded function of the energy monotonously increasing to unity at $s\to\infty$ [40–43]:

$$K_\tau(s) = \int_0^1 dy \frac{y^2(1-y)}{y^2 + s(1-y)/m_\tau^2}. \tag{1.24}$$

The computation gives [17]

$$a_\tau^{\mathrm{HLO}} = 337.5\,(3.7)\cdot 10^{-8}. \tag{1.25}$$

As for the QED three-loop case, the hadronic higher-order contribution (α^3) can be divided into two parts: $a_\tau^{\mathrm{HHO}} = a_\tau^{\mathrm{HHO}}(\mathrm{vp}) + \mathrm{a}_\tau^{\mathrm{HHO}}(\mathrm{lbl})$. The first one arises from diagrams containing hadronic self-energy insertions in the photon propagators and can be estimated as in the leading-order case. The second term is the hadronic light-by-light contribution and cannot be directly determined via a dispersion relation approach. Its evaluation therefore relies on specific models of low-energy hadronic interactions with electromagnetic currents. The latest estimates are $a_\tau^{\mathrm{HHO}}(\mathrm{vp}) = 7.6\,(2)\cdot 10^{-8}$ [44] and $a_\tau^{\mathrm{HHO}}(\mathrm{lbl}) = 5\,(3)\cdot 10^{-8}$ [17]. The

total hadronic contribution is [17]

$$a_\tau^{\rm HAD} = a_\tau^{\rm HLO} + a_\tau^{\rm HHO}({\rm vp}) + {\rm a}_\tau^{\rm HHO}({\rm lbl}) = 350.1(4.8)\cdot 10^{-8}. \tag{1.26}$$

Now we can add up all the discussed terms to derive the SM prediction to a_τ:

$$a_\tau^{\rm SM} = a_\tau^{\rm QED} + a_\tau^{\rm EW} + a_\tau^{\rm HAD}, \tag{1.27}$$

where

$$a_\tau^{\rm QED} = 117\,324\,(2)\cdot 10^{-8}, \tag{1.28}$$

$$a_\tau^{\rm EW} = 47.4\,(5)\cdot 10^{-8}, \tag{1.29}$$

$$a_\tau^{\rm HAD} = 350.1(4.8)\cdot 10^{-8}. \tag{1.30}$$

The final results is

$$a_\tau^{\rm SM} = 117\,721\,(5)\cdot 10^{-8}. \tag{1.31}$$

1.3 New Physics and g-2

Quite generally, New Physics associated with a scale Λ is expected to modify the SM prediction of the anomalous magnetic moment of a lepton l of mass m_l by a contribution of order $a_l^{\rm NP} \sim m_l^2/\Lambda^2$. Therefore, given the large factor $(m_\tau/m_\mu)^2 \sim 283$, the $g-2$ of the τ is much more sensitive than the one of the muon to EW and NP effects which give contribution $\sim m_l^2$, making its measurement an excellent opportunity to unveil or constrain NP effects.

Another interesting feature can be observed comparing the magnitude of EW and hadronic contributions to the muon and τ lepton $g-2$. The EW contribution to the τ magnetic moment is only a factor 7 smaller than the hadronic one, compared to a factor 45 in the case of the muon. Also, while the EW contribution to $a_\mu^{\rm SM}$ is only a factor of 3 larger than the present uncertainty of the hadronic contribution, this factor raises to 10 for the τ lepton. If an NP contribution were of the same order of magnitude as that of the EW, from a purely theoretical point of view, the $g-2$ of the τ would provide a much cleaner test of the presence (or absence) of such NP effects than the muon one. Indeed, if this were the case, such an NP contribution to the τ lepton anomalous magnetic moment could be much larger than the hadronic uncertainty, which is currently the limiting factor of the SM prediction.

1.4 The tau lepton EDM

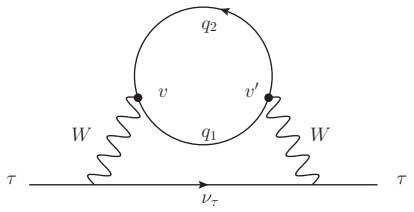

FIGURE 1.5: This two-loop diagrams does not contribute to lepton EDM. The external photon (not shown) can be attached to any charged particle

As already mentioned, the EDM interaction violates CP-invariance. In the SM, with massless neutrinos, the only source of CP violation is the CKM-phase (and a possible θ-term in QCD sector). Therefore, a fundamental lepton EDM arises from virtual quarks coupled to the lepton via virtual $W^{\pm}$. It can be shown [45, 46] that all CP-violating amplitudes are proportional to the phase-convention-independent Jarlskog invariant, J, defined by [46]

$$\mathrm{Im}\left[V_{ij}V_{kl}V_{il}^{*}V_{kj}^{*}\right] = J\sum_{m,n}\varepsilon_{ikm}\varepsilon_{jln}, \tag{1.32}$$

$$J = s_{12}\, s_{13}\, s_{23}\, c_{12}\, c_{13}^{2}\, c_{23}\, \sin(\delta), \tag{1.33}$$

where $s_{ij} = \sin\theta_{ij}$ and $c_{ij} = \cos\theta_{ij}$, θ_{ij} are the three mixing angles of the matrix V_{CKM} as defined in [47], and δ is the KM phase responsible for all CP-violating phenomena in flavor-changing processes in the SM [48].

Naively one might expect a contribution to lepton EDMs from the two-loop diagram of Fig. 1.5. However, for each CKM matrix contribution, V_{ij}, at one vertex v, there is a contribution V_{ij}^{*} at the other vertex v'. Hence the overall amplitude cannot contain a CP-violating phase. Then, one can consider three-loop diagrams. The situation was first analyzed in some detail in [49], but it was subsequently shown that the various contributions from three-loop diagrams (see for example Fig. 1.6) cancel [50], yielding a net contribution of zero in the absence of gluonic corrections to the quark lines. For this reason, in the SM lepton EDMs are predicted to be extremely small, of the $\mathcal{O}(10^{-38} - 10^{-35}\, e{\cdot}\mathrm{cm})$ [51], which is far below the current experimental capabilities.

Models for physics beyond the SM generally induce large contributions to lepton and neutron EDMs, and although there has been no experimental evidence for an EDM so far, there is considerable hope to gain new insights into the nature of CP violation through this kind of experiments.

The current 95% confidence level limits on the EDM of the τ lepton are given by

$$\begin{aligned} -2.2 < \mathrm{Re}(d_\tau) < 4.5 \ \ (10^{-17}\, e\,\mathrm{cm}), \\ -2.5 < \mathrm{Im}(d_\tau) < 0.8 \ \ (10^{-17}\, e\,\mathrm{cm}); \end{aligned} \tag{1.34}$$

they were obtained by the Belle collaboration [19] following the analysis of Ref. [52] for the impact of an effective operator for the τ EDM in the process $e^+e^- \to \tau^+\tau^-$.

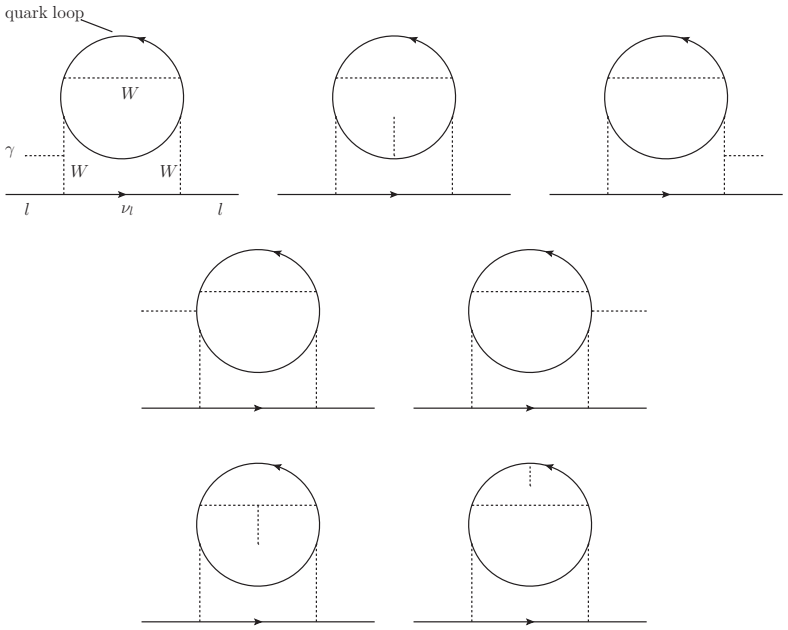

FIGURE 1.6: The sum of contributions to the tau EDM from these three-loop diagrams vanishes in the SM as shown in Ref. [50]. For clarity here the vector boson propagators are draw with dashed lines.

1.5 Experimental determintaion of a_τ

The very short lifetime of tau lepton (2.9×10^{-13} s) makes it very difficult to measure its electric and magnetic dipole moments. the present resolution on its anomalous magnetic moment, a_τ, is only of $\mathcal{O}(10^{-2})$ [16], more than an order of magnitude larger than its SM prediction (1.31). In fact, while the SM value of a_τ is known with a tiny uncertainty of 5×10^{-8} (1.31), this short lifetime has so far prevented the determination of a_τ measuring the tau spin precession in a magnetic field, like in the electron and muon $g-2$ experiments. Instead, in order to investigate the dipole moment form factors, experiments focused on various high-precision measurements of τ pair production in high-energy processes, comparing the measured cross sections with the SM predictions.

The current PDG limit on the tau $g-2$ was derived in 2004 by the DELPHI collaboration from $e^+e^- \to e^+e^-\tau^+\tau^-$ total cross section measurements at $\sqrt{s}$ between 183 and 208 GeV at LEP2 (the study of a_τ via this channel was proposed in [53]). The measured cross-sections were used to extract limits on the anomalous magnetic and electric dipole moments of the tau lepton. The measured values of the cross section were compared to the SM values, assuming that possible deviation were due to non-SM values of a_τ. The 95% CL limit obtained is [16]

$$-0.052 < a_\tau < 0.013, \tag{1.35}$$

that can be also expressed in the form of central value and error as [16]

$$a_\tau = -0.018\,(17). \tag{1.36}$$

In [54] the reanalysis of various measurements of the cross section of the process $e^+e^- \to \tau^+\tau^-$, the transverse τ polarization and asymmetry at LEP and SLD, as well as the decay width $\Gamma(W \to \tau\nu_\tau)$ at LEP and Tevatron allowed the authors to set a model-independent limit on new physics contributions,

$$-0.007 < a_\tau^{\rm NP} < 0.005, \tag{1.37}$$

a bound stronger than that in Eq. (1.35). This analysis, like earlier ones, was performed without radiative corrections, but the authors checked that the inclusion of initial-state radiation did not affect significantly the obtained bounds. However this analysis is not taken into account by the PDG data group because in [54] it is assumed $\mathrm{Im}(a_\tau) = 0$.

Comparing Eqs. (1.31) and (1.36) (their difference is roughly one standard deviation), it is clear that the sensitivity of the best existing measurements is still more than one order of magnitude worse than needed.

Several methods have been suggested to improve upon existing bound. In [55] was suggested to study the radiative decay $W \to \tau\bar{\nu}_\tau\gamma$ as a function of the anomalous magnetic moment of the tau. Authors computed the future statistical bounds achievable at Tevatron and LHC (1 year run) through the study of the normalized differential decay rate for $W \to \tau\bar{\nu}_\tau\gamma$ $(\frac{d\Gamma}{dE_\gamma}/\Gamma_{\rm SM})$. The expected sensitivity at Tevatron and LHC (1 year run) are, respectively, 2.3×10^{-2} and 2.5×10^{-3} at 90% CL (but no background is considered in this analysis).

In [56] was investigated the possibility of using heavy-ion collision at the LHC for measuring the electromagnetic properties of tau lepton. The suggested reaction

$$\mathrm{PbPb} \to \mathrm{PbPb}\,\gamma\gamma \to \mathrm{PbPb}\,\tau\tau \tag{1.38}$$

has the advantage that photons here can be seen as initial partons and therefore almost real ($q^2 \sim 0$). However, in this case, the longitudinal momentum of the $\tau^+\tau^-$ pair cannot be reconstructed. The expected 1σ bounds at the LHC, for the analyzed subchannel $\gamma\gamma \to \tau\tau \to \ell\rho\nu\nu\nu$, is $|a_\tau| < 3 \times 10^{-3}$ [56].

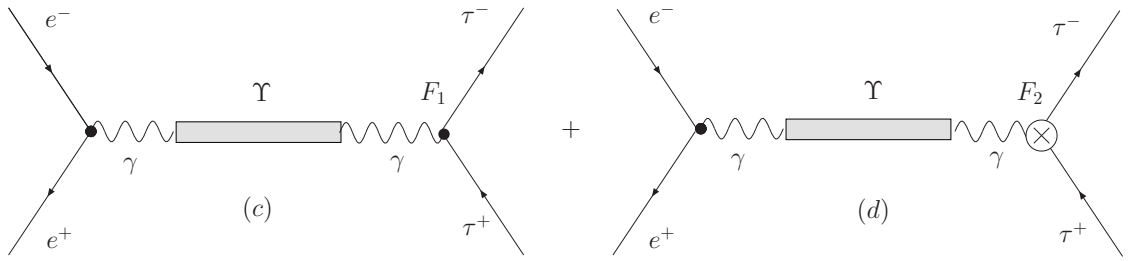

FIGURE 1.7: Diagrams: (c) Υ production, (d) F_{2V} in Υ production.

Yet another method would use the channeling of polarized taus in a bent crystal similarly to the suggestion for the measurement of magnetic moments of short-living baryons [57]. In these kind of experiments, a strong electric field is applied to the bent crystal and properly tuned so that the electric field is seen by the fast-moving particle as a large mega-tesla magnetic field: the spin then precesses significantly before the particle decay, and it can be measured later from the angular distribution of final state particles This method has been successfully tested by the E761 collaboration at Fermilab, which measured the magnetic moment of the Σ^+ hyperon [58]. However the challenge of this method is to produce of a polarized beam of taus. In the case of muon $g-2$ experiment, the polarized muons come from pions that almost totally decay $\pi^+ \to \mu^+\nu_\mu$. In the case of the tau lepton, it was suggested to use the decay $B^+ \to \tau^+\nu_\tau$, which would produce polarized tau leptons [59], however, this particular decay of the B has a very tiny branching ratio of $\mathcal{O}(10^{-4})$. In 1991, when this suggestion was published, the idea seemed completely unlikely. Nonetheless, in the era of B factories, when the decay $B^+ \to \tau^+\nu_\tau$ is already observed by the Belle collaboration [60], the realization of this idea in a dedicated experiment is definitively not excluded.

The future high-luminosity B factory Belle-II [61] offers new opportunities to improve the determination of tau electromagnetic properties. Authors in [15] proposed to determine the Pauli form factor $F_{2V}(q^2)$ of the tau via $\tau^+\tau^-$ production in the e^+e^- collisions at the Υ resonances ($\Upsilon(1S)$, $\Upsilon(2S)$ and $\Upsilon(3S)$) with a sensitivity of $\mathcal{O}(10^{-5})$ or even better. In super B factories the center-of-mass energy is $\sqrt{s} \approx M_{\Upsilon(4S)} \approx 10$ GeV, and therefore

$F_{2V}(q^2)$ is no longer the magnetic anomaly. When attempting to extract the value of F_{2V} from scattering experiments (as opposed to using, say, a background magnetic field) one encounters additional complications due to the contributions of various other Feynman graphs, not related to the magnetic form factor.

In particular in $e^+e^- \to \tau^+\tau^-$ there are contributions not only from the usual s-channel one-loop vertex corrections but also from box diagrams that, by the way, are gauge dependent. The contributions of the latter may interfere in the experimental determination of what we call $F_{2V}(q^2)$, i.e. the magnetic part coming only from the vertex, and should be somehow subtracted out. This may be done either by computing the box contributions and subtracting them from the cross section, or by performing the measurement in a kinematic region where the boxes happen to be numerically subleading. Indeed, the strategy proposed in [15] for eliminating the contamination from the boxes is to measure the observables on top of the Υ resonances; in this kinematic regime the (non-resonant) box diagrams are numerically negligible, and only one loop corrections to the $\gamma\tau\tau$ vertex are relevant (Fig. 1.7).

However, at Belle and future Belle-II the beam energy spread makes it almost impossible to resolve the very narrow peaks of the $\Upsilon(1S, 2S, 3S)$. Indeed, the visible total cross section of resonances is not a perfect Breit-Wigner resonance, but actually the convolution of the theoretical Breit-Wigner cross section with a gaussian spread,

$$\sigma_{\text{vis.}} = \int \sigma(W) \frac{1}{\sqrt{2\pi}\sigma_{\text{beam}}} \exp\left[-\frac{(W - M_\Upsilon)^2}{2\sigma^2_{\text{beam}}}\right] dW, \tag{1.39}$$

where $\sigma_{\text{beam}} \approx 10$ MeV [62] is the systematic beam energy spread at KEKB in the $W = \sqrt{s} = 2E$ scale, and $\sigma(W)$ is the total cross section in the Breit-Wigner approximation:

$$\begin{aligned}\sigma_{ee\to\Upsilon\to\tau\tau}(s) &= 12\pi \frac{\text{Br}(\Upsilon \to ee)\text{Br}(\Upsilon \to \tau\tau)\Gamma^2_{\text{tot}}}{(s - M^2_\Upsilon)^2 + M^2_\Upsilon\Gamma^2_{\text{tot}}} = \sigma_{\text{peak}} \frac{M^2_\Upsilon\Gamma^2_{\text{tot}}}{(s - M^2_\Upsilon)^2 + M^2_\Upsilon\Gamma^2_{\text{tot}}} \\ &\approx \sigma_{\text{peak}}\pi M_\Upsilon\Gamma_{\text{tot}}\delta(s - M^2_\Upsilon) = \sigma_{\text{peak}}\frac{\pi\Gamma_{\text{tot}}}{2}\delta(W - M_\Upsilon).\end{aligned} \tag{1.40}$$

Here we have defined the cross section at peak $\sigma_{\text{peak}} = 12\pi\text{Br}(\Upsilon \to ee)\text{Br}(\Upsilon \to \tau\tau)/M^2_\Upsilon$. The expression for the visible cross section, obtained substituting Eq. (1.40) into Eq. (1.39), is

$$\sigma_{\text{vis.}} = x\,\sigma_{\text{peak}}, \quad \text{with } x = \sqrt{\frac{\pi}{8}}\frac{\Gamma_{\text{tot}}}{\sigma_W}. \tag{1.41}$$

In Tab. 1.3 we compare the visible cross section for these Υ resonances with the non-resonant cross section around the region of the $\Upsilon(4S)$, $\sigma_{\text{non-res.}}(e^+e^- \to \tau^+\tau^-) \approx 4\pi\alpha^2/(3s) \approx 0.92$ nb. There will not be any notable resonant structure in the cross section, but only

Υ	M_Υ [GeV]	Γ_{tot} [keV]	σ_{peak} [nb]	x	$x\frac{\sigma_{\text{peak}}}{\sigma_{\text{non-res.}}}$
$\Upsilon(1S)$	9.46	54	101	3.4×10^{-3}	37%
$\Upsilon(2S)$	10.02	31	56	2.0×10^{-3}	12%
$\Upsilon(3S)$	10.35	20	68	1.3×10^{-3}	9%
$\Upsilon(4S)$	10.58	20×10^3			

TABLE 1.3: Estimated visible cross section at Belle-II for at $e^+e^- \to \Upsilon \to \tau^+\tau^-$.

some distortion of the slope. Therefore, at Belle (and Belle-II) the $\tau^+\tau^-$ events produced with beams at a centre of mass energy $\sqrt{s} = M_\Upsilon$ are mostly due to non-resonant interacition.

1.6 Radiative leptonic τ decays

We propose to measure the dipole moments of tau lepton through its radiative leptonic decays:

$$\tau^- \to l^- \nu_\tau \bar{\nu}_l \gamma, \quad \text{with } l = e, \mu. \tag{1.42}$$

The possibility to set bounds on a_τ via the radiative leptonic τ decays was suggested long ago in [63]. In that article the authors proposed to take advantage of a radiation zero of the LO differential decay rate which occurs when, in the tau rest frame, the final lepton l and the photon are back-to-back, and l has maximal energy. Since a non-standard contribution to a_τ spoils this radiation zero, precise measurements of this phase-space region could be used to set bounds on its value. However, this method is only sensitive to large values of a_τ (at the radiation zero the dependence on non-standard a_τ contributions is quadratic), and preliminary studies with Belle data show no significant improvement of the existing limits (see Sec. 1.11).

The authors of Ref. [54] and [52] have applied effective Lagrangian techniques to study a_τ and d_τ. Our strategy is similar: the energy scale $\sqrt{s} \approx m_\tau$ involved in tau radiative tau decays allow us to study the tau dipole moments introducing, beside the SM Lagrangian, two new effective terms of the form:

$$\mathcal{L}_{\text{eff}} = \mathcal{L}_{\text{SM}} + c_a \frac{e}{4\Lambda}\, \mathcal{O}_a - c_d \frac{i}{2\Lambda}\, \mathcal{O}_d, \tag{1.43}$$

where the operators $\mathcal{O}_{a,d}$ are given by

$$\mathcal{O}_a \;=\; \bar{\tau}\sigma_{\mu\nu}\tau\, F^{\mu\nu}, \quad \mathcal{O}_d \;=\; \bar{\tau}\sigma_{\mu\nu}\gamma_5\tau\, F^{\mu\nu}. \tag{1.44}$$

The scale Λ represents the scale where any kind of physics which is not described by $\mathcal{L}_{\rm SM}$ generates a contribution to the tau's electric or magnetic dipole moment and is therefore larger than the electroweak scale, i.e. $\Lambda > M_Z$. For simplicity we assume the scale Λ to be equal for both operators $\mathcal{O}_{a,d}$, knowing that actually the scale for the EDM is much higher than that for the $g-2$. The contributions from the two effective operators $\mathcal{O}_{a,d}$ to the electromagnetic form factors are the same for $q^2 = 0$ as for $q^2 \neq 0$. The point is that only higher dimensional operators would give rise to a difference between these two cases, which means that such contributions are suppressed by higher powers of q^2/Λ^2 [54]. In our case, q^2 may be of the order of m_τ^2 while Λ is certainly higher than M_Z and we may therefore safely neglect contributions from higher dimensional operators. Of course, the requirement that $q^2 \ll \Lambda^2$ is the fundamental hypothesis of our effective Lagrangian approach.

Even if the set of two operators introduced in Eqs. (1.43) and (1.44) are not gauge invariant under the gauge group $SU(2)_L \times U(1)_Y$, they can be recovered from dimension-six gauge invariant operators,

$$\mathcal{O}_B = \frac{g'}{2\Lambda^2}\bar{\ell}_{\rm L}\phi\,\sigma^{\mu\nu}\tau_{\rm R}B_{\mu\nu} + \text{h.c.}, \tag{1.45}$$

$$\mathcal{O}_W = \frac{g}{2\Lambda^2}\bar{\ell}_{\rm L}t^a\phi\,\sigma^{\mu\nu}\tau_{\rm R}W^a_{\mu\nu} + \text{h.c.}, \tag{1.46}$$

after spontaneous symmetry breaking [64–67]. Here $\ell_{\rm L} = (\nu_{\tau{\rm L}}, \tau_{\rm L})$ is the tau leptonic doublet, ϕ is the Higgs doublet, $B^{\mu\nu}$ and $W^{\mu\nu}$ the $U(1)_Y$ and $SU(2)_L$ field strength tensors, and g' and g are the gauge couplings. However, for simplicity we will consider only the dimension five operators in Eq. (1.43).

The effective Lagrangian in Eq. (1.43) gives the following predictions for the tau dipole moments:

$$a_\tau = \frac{\alpha}{2\pi} + c_a\frac{m_\tau}{\Lambda} + \cdots \tag{1.47}$$

$$d_\tau = c_d\,\frac{1}{\Lambda} + \cdots \tag{1.48}$$

where the dots indicate higher-order contributions not relevant for our discussion (note, in (1.48), that d_τ has no QED contribution). We then define the parameters

$$\tilde{a}_\tau \equiv c_a\frac{m_\tau}{\Lambda}, \quad \tilde{d}_\tau \equiv c_d\,\frac{1}{\Lambda}. \tag{1.49}$$

Our goal is to provide a method to determine $\tilde{a}_\tau$ and $\tilde{d}_\tau$ with a precision of $O(10^{-3})$ or better. This calls for an analogous precision on the theoretical side. For this reason, we computed the decay rate prediction for the processes in (1.42) including radiative

corrections at next-to-leading order (NLO) in QED and not negligible contribution from W-boson propagator of $\mathcal{O}(m_\tau^2/M_W^2) \approx 5 \cdot 10^{-4}$ (see Secs. 1.8 and 1.9). The comparison of this NLO prediction, modified by the additional terms in (1.43), to sufficiently precise data allows to determine $\tilde{a}_\tau$ and $\tilde{d}_\tau$ (and thereby a_τ via (1.47)) possibly down to the level of $O(10^{-4})$. Feasibility study results for the measurement of $\tilde{a}_\tau$ and $\tilde{d}_\tau$ at Belle and Belle-II are then reported in Sec. 1.11

1.7 Muon Decay and the definition of G_F

Before discussing tau leptonic radiative decays, it is worthwhile to recall the relation between muon decay and the definition of the Fermi constant G_F.

Let us focus our attention on muon decay. In the SM, the full inclusive decay rate of

$$\mu^- \to e^- \nu_\mu \bar{\nu}_e(\gamma) \tag{1.50}$$

is [68]

$$\Gamma_{(\mu)} = \frac{G_\mu^2 M^5}{192\pi^3} F\big(r^2\big) \left(1 + \delta_\mu\right) \left[1 + \delta_{\rm W}(M, m)\right], \tag{1.51}$$

where $r = m/M$, $r_{\rm W} = M/M_{\rm W}$,

$$F(t) = 1 - 8t + 8t^3 - t^4 - 12t^2 \ln t \tag{1.52}$$

is a phase-space factor and M and m are, respectively, the muon and electron mass. Also,

$$\frac{G_\mu}{\sqrt{2}} \equiv \frac{g^2}{8M_{\rm W}^2} \left(1 + \Delta r\right), \tag{1.53}$$

where g is the $\mathrm{SU}(2)_L$ gauge coupling constant and Δr is the electroweak correction introduced by Sirlin in Ref. [69]. The term δ_μ is the QED correction evaluated in the Fermi V–A theory; it includes the corrections of virtual and real photons up to $\mathcal{O}(\alpha^2)$, as well as the tiny contribution of the decay $\mu^- \to e^- \nu_\mu \bar{\nu}_e e^+ e^-$ [70–79]. Moreover,

$$\delta_{\rm W}(M, m) = \frac{3}{5} r_{\rm W}^2 \frac{\left(1 - r^2\right)^5}{F(r^2)} + \mathcal{O}\big(r_{\rm W}^4\big) \tag{1.54}$$

is the tree-level correction induced by the W-boson propagator recently computed by Ferroglia, Greub, Sirlin and Zhang [68]. Its leading and next-to-leading contributions can be immediately derived from (1.54): $(3/5)(M/M_{\rm W})^2$ and $(9/5)(m/M_{\rm W})^2$, respectively. While the leading one is well known in the literature [80, 81], the next-to-leading term

differs from that reported in earlier publications [82–84]. We also computed these tree-level correction induced by the W-boson propagator and we confirmed the result in (1.54), in agreement with Ref. [68]. We should add that while $(3/5)(m_\mu/M_{\rm W})^2 \sim 1.0 \times 10^{-6}$ is of the same magnitude as the present experimental relative uncertainty of the muon decay rate in (1.51), 1.0 ppm, the subleading contribution $(9/5)(m_e/M_{\rm W})^2 \sim 7.3 \times 10^{-11}$ is out of experimental reach in the foreseeable future. Moreover, radiative corrections to muon decay of $\mathcal{O}(\alpha^3) \sim 10^{-7}$ and $\mathcal{O}(\alpha\, m_\mu^2/M_{\rm W}^2) \sim 10^{-8}$ have not yet been computed.

The Fermi constant of weak interactions, G_F, is defined from the muon lifetime τ_μ evaluated in the Fermi V–A theory,

$$\mathcal{L} = -\frac{G_F}{\sqrt{2}} \left[\bar{\psi}_{\nu_\mu} \gamma^\alpha (1-\gamma_5)\, \psi_\mu\right] \left[\bar{\psi}_e \gamma_\alpha (1-\gamma_5)\, \psi_{\nu_e}\right] + \text{h.c.}, \tag{1.55}$$

plus QED to leading order in the weak interaction coupling constant. We remind the reader that to leading order in G_F, but to all orders in α, the radiative corrections to muon decay in the Fermi V–A theory are finite after mass and charge renormalization [18]. Specifically, the present Particle Data Group (PDG) definition of G_F is given by the relation [85, 86]

$$\frac{1}{\tau_\mu} = \frac{G_F^2 m_\mu^5}{192\pi^3}\, F\!\left(\frac{m_e^2}{m_\mu^2}\right) (1+\delta_\mu)\,. \tag{1.56}$$

This definition is independent of $M_{\rm W}$, whereas earlier ones (see, for example, PDG 2010 [31]) included the additional factor $[1 + (3/5)m_\mu^2/M_{\rm W}^2]$ on the r.h.s. of (1.56). Since this factor does not arise in the Fermi theory framework, it is more natural not to include it in the definition in (1.56). Also, identifying (1.56) with (1.51) one finds the relation [68]

$$G_\mu^2 = G_F^2/\left[1 + \delta_{\rm W}(m_\mu, m_e)\right], \tag{1.57}$$

with $\delta_{\rm W}(m_\mu, m_e) = 1.04 \times 10^{-6}$ given by (1.54).

The muon decay rate in (1.51) can be immediately extended to the tau leptonic decays

$$\tau^- \to l^-\, \nu_\tau\, \bar{\nu}_l\, (\gamma) \quad \text{with } l = e, \mu, \tag{1.58}$$

identifying M with m_τ and m with m_e or m_μ. The QED correction δ_μ should also be replaced by δ_τ, the appropriate one for these decays, while the electroweak corrections are the same as those contained in G_μ for muon decay [87]. Furthermore, in order to express these tau decay rates in terms of G_F, one should also replace G_μ in (1.51) via (1.57), thus obtaining

$$\Gamma_{(\tau)} = \frac{G_F^2 M^5}{192\pi^3}\, F\big(r^2\big)\, (1+\delta_\tau) \left[\frac{1+\delta_{\rm W}(M,m)}{1+\delta_{\rm W}(m_\mu, m_e)}\right]. \tag{1.59}$$

Note that the leading contribution to $\delta_{\rm W}(M,m)$, appearing in the numerator in square brackets, is independent of the flavor of the final lepton; it amounts to $(3/5)(m_\tau/M_{\rm W})^2 \sim 2.9\times10^{-4}$. The term $\delta_{\rm W}(m_\mu,m_e)$ in the denominator, due to the relation between G_μ and G_F, has been kept for completeness, but it is of the same order of magnitude as the uncomputed radiative corrections of $\mathcal{O}(\alpha\, m_\tau^2/M_{\rm W}^2) \sim 10^{-6}$. The hadronic corrections to (1.59) are still missing too; they are of $\mathcal{O}(\alpha^2/\pi^2) \sim 10^{-5}$ [76, 88].

Our prediction for the energy-angle distribution of the final charged lepton in the decays (1.50) and (1.58) of a polarized μ^- or τ^- at rest is

$$\begin{aligned}\frac{d^2\Gamma_{(\mu,\tau)}}{dx\, d\cos\theta_l} = \frac{G_F^2 M^5}{192\pi^3}\frac{x\beta}{1+\delta_{\rm W}(m_\mu,m_e)}\times\\ \big\{3x-2x^2+r^2(3x-4)+f(x)\\ +r_{\rm W}^2\big[2x^2-x^3-2r^2\big(1+x-x^2+r^2\big)\big]\\ -\cos\theta_l\; x\beta\,\big[2x-1-3r^2+g(x)\\ +r_{\rm W}^2\,x\,\big(x-2r^2\big)\big]+\mathcal{O}\big(r_{\rm W}^4\big)\big\}\,,\end{aligned} \tag{1.60}$$

where $\beta\equiv|\vec{p}_l|/E_l=\sqrt{1-4r^2/x^2}$, $p_l=(E_l,\vec{p}_l)$ is the four-momentum of the final charged lepton, $x=2E_l/M$ varies between $2r$ and $1+r^2$, p and $n=(0,\hat{n})$ are the four-momentum and polarization vector of the initial muon or tau, with $n^2=-1$ and $n\cdot p=0$, and $\cos\theta_l$ is the angle between $\hat{n}$ and $\vec{p}_l$. The corresponding formula for the decay of a polarized μ^+ or τ^+ is simply obtained inverting the sign in front of $\cos\theta_l$ in (1.60).

The functions $f(x)$ and $g(x)$ are the QED radiative corrections; $f(x)$, contributing to the isotropic (θ_l-independent) part, has been calculated up to $\mathcal{O}(\alpha^2)$, while $g(x)$, contributing to the anisotropic one, is known up to leading $\mathcal{O}(\alpha^2)$ effects [70–73, 89–94]. The hadronic corrections to (1.60), which are of $\mathcal{O}(\alpha^2/\pi^2)$, were computed for the decay of the muon, but not yet for the tau [95]. The terms proportional to $r_{\rm W}^2$ are induced by the W-boson propagator. The leading ones, of $\mathcal{O}(r_{\rm W}^2)$, agree with those of Ref. [96]. To our knoledge, the calculation of the subleading terms, of $\mathcal{O}(r^2 r_{\rm W}^2)$, is new.

1.8 Radiative tau decays: Tree-level contributions

We can now turn our attention to the decays

$$\tau^-\to l^-\bar{\nu}_l\nu_\tau\gamma,\quad \text{with } l=e,\mu, \tag{1.61}$$

where the photon is detected and measured.

The SM leading-order (LO) prediction for the differential decay rate in Eq. (1.61) of a polarized τ^- is, in the tau lepton rest frame,

$$\frac{d^6\Gamma^0}{dx\,dy\,d\Omega_l\,d\Omega_\gamma} = \frac{\alpha G_F^2 M^5}{(4\pi)^6}\frac{x\beta}{1+\delta_{\rm W}(m_\mu,m_e)} \times \Big[G(x,y,c) + x\,\beta\,\hat{n}\cdot\hat{p}_l\,J(x,y,c) \;+ y\,\hat{n}\cdot\hat{p}_\gamma\,K(x,y,c)\Big], \tag{1.62}$$

where $\alpha = 1/137.035\,999\,174\,(35)$ [97] is the fine-structure constant, $G_F = 1.166\,378\,7(6)\times 10^{-5}$ GeV^{-2} [98] is the Fermi coupling constant, $m_\tau = 1.776\,82\,(16)$ GeV [85] and $r = m_l/m_\tau$. Also $x = 2E_l/M$ and $y = 2E_\gamma/M$, where E_l and E_γ are the energy of l and photon. The final charged lepton and photon are emitted at solid angles Ω_l and Ω_γ, respectively, with normalized three-momenta $\hat{p}_l$ and $\hat{p}_\gamma$, and $c \equiv \cos\theta$ is the cosine of the angle between $\hat{p}_l$ and $\hat{p}_\gamma$. The corresponding formula for the radiative decay of a polarized τ^+ (or μ^+) is simply obtained inverting the signs in front of the scalar products $\hat{n}\cdot\hat{p}_l$ and $\hat{n}\cdot\hat{p}_\gamma$ in (1.62).

The function G and, analogously, J and K, are given by

$$G(x,y,c) = \frac{4}{3yz^2}\Big[g_{\rm LO}(x,y,z) \;+\; r_{\rm W}^2\,g_{\rm W}(x,y,z) + \mathcal{O}\big(r_{\rm W}^4\big)\Big], \tag{1.63}$$

where $z = xy\,(1-c\beta)\,/2$. The functions $g_{\rm LO}$, $j_{\rm LO}$, and $k_{\rm LO}$, computed in [72, 81, 99, 100], arise from the pure Fermi V–A interaction, whereas $g_{\rm W}$, $j_{\rm W}$, and $k_{\rm W}$ are the new leading contributions of the W-boson propagator. Their explicit expressions are reported in Appendix.

The operators $\mathcal{O}_a$ and $\mathcal{O}_d$ in Eq. (1.43) generate additional contributions to the differential decay rate in (1.62). They can be summarised in the shift

$$G(x,y,c) \;\to\; G(x,y,c) \;+\; {\rm Re}(\tilde{a}_\tau)\,G_a(x,y,c) \;+\; m_\tau\,{\rm Im}(\tilde{d}_\tau)\,G_d(x,y,c), \tag{1.64}$$

and similarly for J and K. Moreover, inside the squared bracket of Eq. (1.62) it appears the additional term

$$y\,x\,\beta\,\vec{n}\cdot(\hat{p}_l\times\hat{p}_\gamma)\,\Big[m_\tau\,{\rm Re}(\tilde{d}_\tau)\,L_d(x,y,c) + {\rm Im}(\tilde{a}_\tau)\,L_a(x,y,c)\Big] \tag{1.65}$$

inside the square brackets of (1.62). Tiny terms of $O(\tilde{a}^2)$ and $O(\tilde{d}^2)$ were neglected since known to be subleading.

1.9 Radiative tau decays: QED radiative corrections

As shown long ago by Sirlin in [18], to leading order in G_F but to all orders in α, the radiative corrections to muon decay are finite in the Fermi V-A theory.Since this special feature holds also for taus decaying into leptons, we computed all NLO corrections to radiative leptonic decays in the Fermi theory, i.e. collapsing the weak decay, mediated by the W-boson, to an effective four-fermion interaction. This is sufficient for the desired level of precision: higher order NLO correction are expected to of $\mathcal{O}(\alpha\, m_\tau^2/M_W)$. In this section we present our NLO prediction originated by real photon emission and one-loop virtual photonic corrections. Our results will be also compared with previous works [101, 102] Throughout the calculation, full dependence on the mass ratio $r = m_r/m_\tau$ is taken into account.

1.9.1 Virtual corrections

In the Fermi theory the exchange of a W boson in tau decays is collapsed to a four-fermion interaction. Therefore a virtual photon can be exchanged only between charged fermion, as shown in Fig. 1.8. We performed the computation of one-loop diagrams via Passarino-Veltman reduction [103] of tensor integral, with the use of the *Mathematica* package `FeynCalc` [104] as well as `Form` [105] for the algebra of gamma matrices. We calculated the final set of scalar integrals as described in [106] and we numerically checked our results with `LoopTools` [107]. We also used results of Ref. [108] for box scalar integrals appearing from diagrams in Fig. 1.8d. We adopted dimensional regularization, in order to regularize ultraviolet divergences (UV), and we introduced a fictitious photon mass, λ, for the treatment of infrared divergences (IR) related to soft photon emission. IR singularities associated to collinear photon emission were already "regularized" since we kept the final charged lepton mass dependence. UV divergences were removed via on-shell renormalization scheme.

After mass and charge renormalization UV divergences cancel out in the case of tau and muon decay [69], contrary to what append in general in the Fermi theory. This follows from the fact that, under a Fierz rearrangement that interchanges the wave functions ψ_e and ψ_{ν_μ} in Eq. (1.55), the currents remain purely left-handed vector currents. This is in sharp contrast to the case of neutron decay in which scalar and pseudo-scalar terms are generated and for which the following arguments break down. The radiative corrections in that case are not finite.

Considering the vector part, $\bar{\psi}_e\gamma^\mu\psi_\mu$, of this effective $\mu - e$ current, one sees that after fermion mass renormalization is performed the remaining divergences are independent of

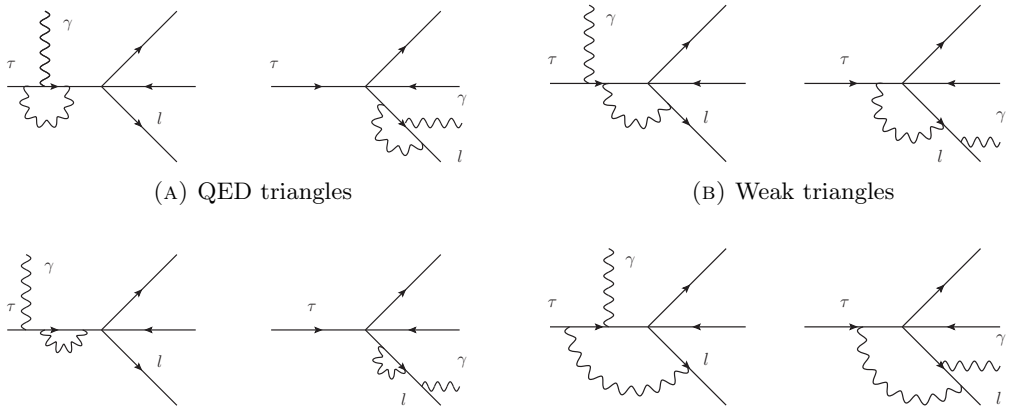

(A) QED triangles (B) Weak triangles

(C) Selfenergies (D) Boxes

FIGURE 1.8: Tau radiative decays: one loop diagrams.

the masses and thus cancel, as for the case of pure QED. The QED corrections to the axial vector part may be shown to be finite by noting that the transformations $\psi_e \to \gamma_5 \psi_e$ and $m_e \to -m_e$ leave $\mathcal{L}_{\text{QED}}$ invariant but exchange $\bar{\psi}_e \gamma^\alpha \psi_\mu \leftrightarrow \bar{\psi}_e \gamma^\alpha \gamma_5 \psi_\mu$. Thus the radiative corrections to the axial-vector part of the current are equal to those of the vector part in the limit of $m_e = 0$.

In practice, if we express the Fermi Lagrangian expressed in term of bare fields as

$$-\frac{G_F}{\sqrt{2}} \bar{\nu}_{0\tau} \left[\gamma^\mu (1-\gamma^5)\right] \tau_0 \cdot \bar{l}_0 \left[\gamma_\mu (1-\gamma^5)\right] \nu_{0l} + \text{h.c.}, \tag{1.66}$$

renormalization of the wave functions, $\tau_0 = \sqrt{Z_{2\tau}}\tau$ and $l_0 = \sqrt{Z_{2l}} l$, leads to

$$-\frac{G_F}{\sqrt{2}} \sqrt{Z_{2\tau}} \sqrt{Z_{2l}} \bar{\nu_\tau} \left[\gamma^\mu (1-\gamma^5)\right] \tau \cdot \bar{l} \left[\gamma_\mu (1-\gamma^5)\right] \nu_l + \text{h.c.}. \tag{1.67}$$

The renormalization condition of muon decay does not required the introduction of a bare G_F. By expanding to the first order in α the factor $\sqrt{Z_{2\tau}}\sqrt{Z_{2l}}$,

$$\sqrt{Z_{2\tau}}\sqrt{Z_{2l}} = 1 + \frac{1}{2}(\delta Z_{2\tau} + \delta Z_{2l}) + O(\alpha^2), \tag{1.68}$$

we can identify the second term of the r.h.s. as a sort of "counter term", which exactly cancel the UV divergences in diagrams 1.8b. However, we stress that this cancellation is accidental in muon decay and it is not imposed by any renormalization condition as in the case of charge or mass.

1.9.2 Real corrections

Emission of a second soft photon with energy below some threshold is experimentally undistinguishable from single emission. If the soft energy-cut satisfies $E_{\min} \ll m_\tau$, then the total amplitude factorizes:

$$\mathcal{M}_{\gamma\gamma} = ie\left[\frac{p_l\cdot\varepsilon'}{p_l\cdot k'} - \frac{p_\tau\cdot\varepsilon'}{p_\tau\cdot k'}\right]\mathcal{M}_\gamma, \tag{1.69}$$

where ε' and k' are polarization and momentum of the second soft photon, and $\mathcal{M}_\gamma$ is the LO amplitude for the single photon emission. Integration over the soft photon phase space gives

$$\begin{aligned} d\Gamma_{\gamma\gamma} = -\frac{\alpha}{\pi}\Bigg\{&\left(\ln y_{\min}^2 - \ln\frac{\lambda^2}{M^2}\right)\left[1+\frac{x}{\sqrt{x^2-4r^2}}\ln\left(\mathcal{X}_1\right)\right] \\ &+\frac{x}{\sqrt{x^2-4r^2}}\left[\ln^2\left(\mathcal{X}_1\right)+\ln\left(\mathcal{X}_1\right)+\mathrm{Li}_2\left(\frac{2\sqrt{x^2-4r^2}}{x+\sqrt{x^2-4r^2}}\right)\right]-1\Bigg\}\,d\Gamma_\gamma. \end{aligned} \tag{1.70}$$

where $y_{\min} = 2E_{\min}/m_\tau$ is the normalized photon energy threshold, λ is the fictitious photon mass and

$$\mathcal{X}_1 = -\frac{x-2r-\sqrt{x^2-4r^2}}{x-2r+\sqrt{x^2-4r^2}}. \tag{1.71}$$

Our result in Eq. (1.70) agrees with those in Refs. [72, 102]. In the end, we verified that IR poles arising from virtual correction cancel out with those appearing in real photon emission.

1.9.3 NLO prediction and comments

The differential decay rate for $\tau \to l\nu_\tau\bar{\nu}_l\gamma$ at NLO in QED is

$$\begin{aligned} \frac{d^6\Gamma}{dx\,dy\,d\Omega_l\,d\Omega_\gamma} = \frac{\alpha\,G_F^2M^5}{(4\pi)^6}\frac{x\beta}{1+\delta_{\rm W}(m_\mu,m_e)}\Bigg[&G(x,y,c)+x\beta\,\hat{n}\cdot\hat{p}_l\,J(x,y,c) \\ &+y\,\hat{n}\cdot\hat{p}_\gamma\,K(x,y,c)+y\,x\beta\,\hat{n}\cdot(\hat{p}_l\times\hat{p}_\gamma)\,L(x,y,c)\Bigg]. \end{aligned} \tag{1.72}$$

The function $G(x,y,c)$, and similarly for J and K, is given by

$$G(x,y,c) = \frac{4}{3yz^2}\left[g_{\rm LO}(x,y,z)+\frac{\alpha}{\pi}\,g_{\rm NLO}(x,y,z;y_{\min})+r_{\rm W}^2\,g_{\rm W}(x,y,z)\right], \tag{1.73}$$

where $g_{\rm LO}(x,y,z)$ and $g_{\rm W}(x,y,z)$ are tree-level contributions, as described before in Sec. 1.8, and $g_{\rm NLO}(x,y,z;y_{\min})$ contains both virtual and real QED corrections. For clarity here, we

omitted those terms involving the dipole moments. The term $L(x, y, z)$, appearing in front of the P violating term $\hat{n}\cdot(\hat{p}_l \times \hat{p}_\gamma)$, is purely induced by loop corrections and free of any IR of UV divergences. As a matter of fact, $L(x, y, z)$ is of the form $\sum_i P_i(x, y, z)\mathrm{Im}\,[I_i(x, y, z)]$, where P_i are polynomials in x, y, z and $I_i(x, y, z)$ are scalar integrals with imaginary part does different from zero.

QED one-loop corrections to muon (tau) leptonic radiative decay were computed before in an unpublished study by Donnachie and Mohammad [109], by Fischer *et al.* in [101], but only the isotropic part $g_{\rm NLO}$ independent on $\hat{n}$, and by Arbuzov and Sherbakova in [102], with full spin dependence, but in the $r \to 0$ limit. While in the first two cases their the results were unavailable, in the second case the authors provided us with the decay rate in a Fortran program. We found perfect numerical agreement for the isotropic part $g_{\rm NLO}$ (better than per mil level), while we totally differ in the anisotropic parts $j_{\rm NLO}$ and $k_{\rm NLO}$. We recall that our calculation has been performed independently by M. Passera, L. Mercolli and M. Fael, and we found agreement for the function $g_{\rm NLO}, j_{\rm NLO}$ and $k_{\rm NLO}$. Moreover, we noted also in the NLO decay rate formula of [102] (equivalent to our expression (1.72)), that the term $L(x, y, z)$ does not appear and thus represent another big discrepancy. From the discussion before, it is clear that the $L(x, y, z)$ may vanishes if one erroneously assumes the scalar integrals to be real. In order to solve this disagreement, or to better confirm our result, we examined in depth our calculation and we performed the following series of check:

- We checked that the function $L(x, y, z)$ is not zero, neither it vanishes in the limit $r \to 0$.
- Since our expression agrees with [102] for the isotropic part G, but not with the spin-dependent one, J, K and L, this suggests that a possible mistake does not lie in the one-loop amplitude computation, but more likely in the evaluation of gamma matrices traces. Anyway, as a main check, we also explicitly verified that the renormalized one-loop amplitude, $\varepsilon^*_\mu(p_\gamma)\mathcal{M}^\mu_{\rm virt}$, satisfy the Ward identity,

$$p_{\gamma\,\mu}\mathcal{M}^\mu_{\rm virt} = 0, \tag{1.74}$$

  where $\epsilon^*_\mu(p_\gamma)$ is the polarization vector of the out coming photon whose momentum is p_γ.
- The traces of gamma matrices have been checked with the programs `Form` and `FeynCalc`.
- Weak decays and spin projectors involve the treatment of γ_5 in dimensional regularization. We used [110] scheme. Another way to treat consistently the γ_5 is to

renounce dimensional regularization. Indeed, since we had to deal only with one-loop integrals, it appeared worthwhile to newly derive the NLO sector of (1.72) in the $D = 4$ Pauli-Villars regularization scheme. We found perfect agreement with the case of dimensional regularization.

1.10 Branching Ratios

In this section we report results for the branching ratios of tau leptonic decays. We implemented the NLO differential decay rates in Eq. (1.72) in C and Fortran codes, used in the feasibility study of Sec. 1.11 and for evaluation of partial widths.

The kinematic limits for x, c, and y are

$$2r \le x \le 1 + r^2, \quad -1 \le c \le 1, \tag{1.75}$$

$$0 < y \le y_{\max}(x, c), \tag{1.76}$$

where the maximum normalized photon energy is

$$y_{\max}(x, c) = \frac{2\,(1 + r^2 - x)}{2 - x + c\,x\beta}. \tag{1.77}$$

However, every experimental setup has a minimum photon energy $E_\gamma^{\min} = y_{\min}(M/2)$ below which photons are not detected. As the constraint $y_{\min} < y_{\max}(x, c)$, necessary to measure radiative decays, leads to the bound $c < c_{\max}(x)$, with

$$c_{\max}(x) = \frac{2\,(1 + r^2 - x) - (2 - x)\,y_{\min}}{x\beta\,y_{\min}}, \tag{1.78}$$

the kinematic ranges of x, c, and $y > y_{\min}$ are reduced to

$$2r \le x \le 1 + r^2, \quad -1 \le c \le \min\{1, c_{\max}(x)\}, \tag{1.79}$$

$$y_{\min} \le y \le y_{\max}(x, c). \tag{1.80}$$

We noted that the terms in G, J, and K proportional to r^2 cannot be neglected in the integrated decay rate. Indeed, the functions multiplying these r^2 terms generate a singular behavior in the $r \to 0$ limit after the integration over $c \equiv \cos\theta$: terms proportional to r^2/z^2 in G (or J, K) lead to a nonvanishing contribution to the integrated decay rate since $\int dc\,(1/z^2) \propto 1/z$ is evaluated at the integration limit $c \to 1$ where $z \to xy\,(1 - \beta)/2 \approx$

process	B.R. 10^{-2}	exp. B.R.
$\mu^+ \to e^+\nu_e\bar{\nu}_\mu\gamma$	1.3×10^{-2}	$1.4\,(4) \times 10^{-2}$
$\tau^- \to e^-\bar{\nu}_e\nu_\tau\gamma$	1.84×10^{-2}	$(1.75 \pm 0.06 \pm 0.17) \times 10^{-2}$
$\tau^- \to \mu^-\bar{\nu}_\mu\nu_\tau\gamma$	3.67×10^{-2}	$(3.61 \pm 0.16 \pm 0.35) \times 10^{-2}$

TABLE 1.4: Branching ration of radiative *mu* and tau decays for a photon energy threshold $E_\gamma^{\min} = 10$ MeV. Experimental value for the decay of μ^+ from ref. [114]. A new preliminary measurement of this branching ratio has recently been reported by the MEG experiment [117]. The values for τ^- were measured by the CLEO Collaboration, where the first error is statistical and the second one is systematic [115].

process	B.R. (LO)	B.R. (NLO)	B.R. (NLO)/B.R. (LO)
$\mu^+ \to e^+\nu_e\bar{\nu}_\mu\gamma$	1.31×10^{-2}	-1.1×10^{-4}	-0.8%
$\tau^- \to e^-\bar{\nu}_e\nu_\tau\gamma$	1.836×10^{-2}	-1.83×10^{-3}	-10%
$\tau^- \to \mu^-\bar{\nu}_\mu\nu_\tau\gamma$	3.67×10^{-2}	-9.1×10^{-4}	-2.5%

TABLE 1.5: Contributions to the branching ratios given by the NLO correction $(\alpha/\pi)g_{\rm NLO}$ in (1.73), and ratios to the LO.

$r^2(y/x)$ for $x \gg 2r$. If the initial $\mu^\pm$ or $\tau^\pm$ are not polarized, Eq. (1.72) simplifies to

$$\frac{d^3\Gamma}{dx\,dc\,dy} = \frac{\alpha G_F^2 M^5}{(4\pi)^6} \frac{8\pi^2\, x\beta}{1+\delta_{\rm W}(m_\mu, m_e)}\, G(x,y,c). \tag{1.81}$$

Integrating Eq. (1.81) over the kinematic ranges (1.79) and dividing the result by the muon or tau total widths $\Gamma_{\mu,\tau}$ one obtains the branching ratios of the radiative decays (1.61) for a given threshold $y_{\min}$. We note that these branching ratios contain mass singularities (and $\ln y_{\min}$) [81, 111], but their presence does not contradict the Kinoshita–Lee–Nauenberg theorem, which applies only to total decay rates [72, 112, 113].

The branching ratio of radiative μ and tau decays with a minimum detected photon energy $E_\gamma^{\min} = 10$ MeV are reported in Tab. 1.4 and compared with current experimental values [114, 115]. Montecarlo integration has been performed with the `Cuba` library [116].

The relative contributions to the branching ratios arising from the isotropic terms $g_{\rm LO}, g_{\rm W}$ and $g_{\rm NLO}$ are shown in Tabs. 1.5 and 1.6. In tau radiative decays, NLO term gives a -10% correction, for $l = e$, and -2.5% correction, for $l = \mu$, and thus cannot be neglected in the measurements of tau dipole moments. These corrections receive enhancement from soft and collinear emission through the logarithms $\ln y_{\min}$ and $\ln r$. Effects from W-boson propagator quite small, of $\mathcal{O}(10^{-4})$. However, we want to emphasize that the lack of these contributions in the decay rate, even if small, would induce an extra source of systematic uncertainty in our analysis.

process	B.R. (LO)	B.R. ($M_{\rm W}$)	B.R. ($M_{\rm W}$)/ B.R. (LO)
$\mu^+ \to e^+\nu_e\bar{\nu}_\mu\gamma$	1.31×10^{-2}	1.5×10^{-8}	$\mathcal{O}(10^{-6})$
$\tau^- \to e^-\bar{\nu}_e\nu_\tau\gamma$	1.836×10^{-2}	5.7×10^{-6}	3×10^{-4}
$\tau^- \to \mu^-\bar{\nu}_\mu\nu_\tau\gamma$	3.67×10^{-3}	1.2×10^{-6}	3×10^{-4}

TABLE 1.6: Contributions to the branching ratios given by the W-boson effect $r_{\rm w}^2 g_{\rm w}$ in (1.73), and ratios to the LO.

Contributions to the partial widths arising from the effective operators (1.44) are very tiny compared to the LO. For example the additional contributions from $g-2$ coupling to the branching ratios are $[(8.6 \times 10^{-4})\tilde{a}_\tau + (3.5 \times 10^{-4})\tilde{a}_\tau^2]\%$ (for $l = e$) and $[(8.2 \times 10^{-4})\tilde{a}_\tau + (3.3 \times 10^{-4}))\tilde{a}_\tau^2]\%$ (for $l = \mu$). Branching ratios are too inclusive quantities to improve upon current bound on tau dipole moments since their contributions are killed by integration. Only exploiting the full phase space one can disentangle these tiny effects. Indeed, the method of unbinned maximum likelihood, described in the next section, basically fits the triple differential decay rate in Eq. (1.72), i.e. it aims precisely to use the maximum amount of information from every single radiative decay event.

1.11 Feasibility study at Belle and Belle-II

by S. I. Eidelman, D. A. Epifanov

As it was suggested in [63] we performed feasibility study of the $\tilde{a}_\tau$ in the vicinity of the radiation zero point in the phase space of $\tau \to \ell\nu\nu\gamma$ ($\ell = e,\ \mu$) decay ($\cos\widehat{(\ell,\gamma)} = -1,\ x = 2E_\ell^{\rm max}/m_\tau = 1 + \frac{m_\ell^2}{m_\tau^2}$). For that we analyzed a set of $\tau^+\tau^-$ events, where one τ decays to the radiative leptonic mode and the other τ decays to ordinary leptonic mode, ($\tau^\pm \to \ell_1^\pm\nu\nu\gamma,\ \tau^\mp \to \ell_2^\mp\nu\nu$), $\ell_{1,2} = e, \mu;\ \ell_1 \neq \ell_2$, or shortly ($\ell_1^\pm\gamma,\ \ell_2^\mp$). We excluded ($e^\pm\gamma,\ e^\mp$) and ($\mu^\pm\gamma,\ \mu^\mp$) events from our analysis due to the large background from $e^+e^- \to e^+e^-\gamma$ and $e^+e^- \to \mu^+\mu^-\gamma$ processes. Analyzed events were produced by KKMC/TAUOLA/PHOTOS generators [118–120] and processed by GEANT3 based program [121] in the conditions of Belle experiment [122–125].

The sensitivity to $\tilde{a}_\tau$ is determined by the background suppression power $\varepsilon_{\rm sig}/\varepsilon_{\rm bg}$ (where: $\varepsilon_{\rm sig}$ - detection efficiency for signal events, $\varepsilon_{\rm bg}$ - detection efficiency for background events). The main background comes from the ordinary radiative leptonic decays (characterized by $\tilde{a}_\tau = 0$) as well as from $(\tau^+ \to \ell_1^+\nu\nu;\ \tau^- \to \ell_2^-\nu\nu)\gamma_{\rm ISR}$ events with initial state radiation (ISR) to the large polar angles in the detector. As the fraction of the signal events in the vicinity of the radiation zero point is very small we extended signal region to maximize

$\varepsilon_{\rm sig}/\varepsilon_{\rm bg}$:

$$0.1 < \cos\widehat{(\ell_1,\gamma)} < 0.8, \quad \cos\widehat{(\ell_2,\gamma)} < -0.9, \quad \text{and } E_\gamma > 0.5 \text{ GeV}. \tag{1.82}$$

Even in this case the $\tilde{a}_\tau$ upper limit (UL($\tilde{a}_\tau$)), which can be achieved with the whole Belle statistics (of about 0.9×10^9 τ pairs) is only UL($\tilde{a}_\tau$) $\simeq 2$. We found that the phenomenon of radiation zero has no large influence on the $\varepsilon_{\rm sig}/\varepsilon_{\rm bg}$. The dynamical structure of the signal events, determined by $G_a(x,y,c)$ and $G_{aa}(x,y,c)$ form factors, allows us to achieve $\varepsilon_{\rm sig}/\varepsilon_{\rm bg} \sim 100$ only. At the same time the suppression of the signal branching fraction (for $\tilde{a}_\tau = 1$) is $\mathcal{B}_{\rm bg}/\mathcal{B}_{\rm sig} \simeq 2000$, i.e. about one order of magnitude larger than $\varepsilon_{\rm sig}/\varepsilon_{\rm bg}$. As a result there is no possibility to improve essentially $\tilde{a}_\tau \sim 1$ sensitivity.

The other more complicated and most powerful method to extract $\tilde{a}_\tau$ and $\tilde{d}_\tau$ is an unbinned maximum likelihood fit of events in the full phase space. The main idea of this method is to consider events where both taus decay to the particular final states. One $\tau^\mp$ (signal side) decays to radiative leptonic mode and the other $\tau^\pm$ (tag side) decays to some well investigated mode with large branching fraction. As a tag decay mode we choose $\tau^\pm \to \rho^\pm\nu \to \pi^\pm\pi^0\nu$, it also serves as spin analyser, which allows us to be sensitive to the spin dependent part of the differential decay width of signal decay using effect of spin-spin correlation of taus [126]. In the technique we analyze ($\ell^\mp\nu\nu\gamma,\ \pi^\pm\pi^0\nu$) events in the 12th dimensional phase space (PS). The probability density function (PDF) is constructed from the total differential cross section $\frac{d\sigma}{\rm dPS}(e^+e^- \to \tau^\mp\tau^\pm \to (\ell^\mp\nu\nu\gamma,\ \pi^\pm\pi^0\nu))$, which is a sum of spin independent term and spin-spin correlation term.

To write the total differential cross section we follow the approach developed in [127, 128]. The differential cross section of $e^+e^- \to \tau^+(\vec{\zeta}^{*+})\tau^-(\vec{\zeta}^{*-})$ reaction in the center-of-mass system (c.m.s.) is given by formula [126]

$$\frac{d\sigma(\vec{\zeta}^{*-},\vec{\zeta}^{*+})}{d\Omega} = \frac{\alpha^2}{64E_\tau^2}\beta_\tau(D_0 + D_{ij}\zeta_i^{*-}\zeta_j^{*+}), \tag{1.83}$$

where $D_0 = 1 + \cos^2\theta + \sin^2\theta/\gamma_\tau^2$ and

$$D_{ij} = \begin{pmatrix} (1+\frac{1}{\gamma_\tau^2})\sin^2\theta & 0 & \frac{1}{\gamma_\tau}\sin 2\theta \\ 0 & -\beta_\tau^2\sin^2\theta & 0 \\ \frac{1}{\gamma_\tau}\sin 2\theta & 0 & 1+\cos^2\theta - \frac{1}{\gamma_\tau^2}\sin^2\theta \end{pmatrix}, \tag{1.84}$$

with $\vec{\zeta}^{*\mp}$ is polarisation vector of $\tau^\mp$ in the $\tau^\mp$ rest frame (unitary vector along $\tau^\mp$ spin direction). Asterisk marks parameters measured in the associated τ rest frame. Moreover, α, E_τ, $\gamma_\tau = E_\tau/M_\tau$, $\beta_\tau = P_\tau/E_\tau$ and θ are fine structure constant, energy, Lorentz factor, velocity of τ (in the units of c) and polar angle of τ^- momentum direction respectively.

Signal differential decay width is written in the form (with unimportant, for this analysis, total normalization constant $\kappa_{\ell\gamma}$):

$$\frac{d\Gamma(\tau^{\mp}(\vec{\zeta}^*) \to \ell^{\mp}\nu\nu\gamma)}{dx^* dy^* d\Omega_\ell^* d\Omega_\gamma^*} = \kappa_{\ell\gamma}\left[A(x^*, y^*, z^*) \mp \vec{\zeta}^* \cdot \vec{B}(x^*, y^*, z^*))\right], \tag{1.85}$$

where $A(x, y, z) = G(x, y, z)$ and

$$\vec{B} = \vec{n}_\ell^* \sqrt{x^{*2} - 4r^2} J + \vec{n}_\gamma^* y^* K + [\vec{n}_\ell^* \times \vec{n}_\gamma^*] y^* x^* \beta^* L \tag{1.86}$$

Definitions of all variables in the last equations can be found in(1.62).

The $\tau^{\pm}(\vec{\zeta'}^*) \to \rho^{\pm}(K^*)\nu(q^*) \to \pi^{\pm}(p_1^*)\pi^0(p_2^*)\nu(q^*)$ decay width reads (with the total normalization constant κ_ρ):

$$\frac{d\Gamma(\tau^{\pm} \to \pi^{\pm}\pi^0\nu)}{dm_{\pi\pi}^2 d\Omega_\rho^* d\tilde{\Omega}_\pi} = \kappa_\rho(A' \mp \vec{B}'\vec{\zeta'}^*) W(m_{\pi\pi}^2), \tag{1.87}$$

where

$$\begin{aligned}
A' &= 2(q, Q)Q_0^* - Q^2 q_0^*, & \vec{B}' &= Q^2 \vec{K}^* + 2(q, Q)\vec{Q}^*, \\
Q^* &= p_1^* - p_2^*, & K^* &= p_1^* + p_2^*, \\
W(m_{\pi\pi}^2) &= |F_\pi(m_{\pi\pi}^2)|^2 \frac{p_\rho(m_{\pi\pi}^2)\tilde{p}_\pi(m_{\pi\pi}^2)}{M_\tau m_{\pi\pi}}, & m_{\pi\pi}^2 &= K^{*2}, \\
p_\rho &= \frac{M_\tau}{2}\left(1 - \frac{m_{\pi\pi}^2}{M_\tau^2}\right), & \tilde{p}_\pi &= \frac{\lambda^{\frac{1}{2}}(m_{\pi\pi}, m_\pi, m_{\pi^0})}{2m_{\pi\pi}}.
\end{aligned} \tag{1.88}$$

Here we used the Källen function $\lambda(x, y, z) \equiv x^2 + y^2 + z^2 - 2xy - 2xz - 2yz$. Also p_ρ and Ω_ρ^* are momentum and solid angle of ρ meson in the τ rest frame, $\tilde{p}_\pi$ and $\tilde{\Omega}_\pi$ the momentum and solid angle of charged pion in the ρ rest frame, and $F_\pi(m_{\pi\pi}^2)$ is pion form factor with CLEO parameterisation [129]. As a result the total differential cross section for $(\ell^{\mp}\gamma, \rho^{\pm})$ events can be written as [126]:

$$\frac{d\sigma(\ell^{\mp}\gamma, \rho^{\pm})}{dE_\ell^* d\Omega_\ell^* dE_\gamma^* d\Omega_\gamma^* d\Omega_\rho^* dm_{\pi\pi}^2 d\tilde{\Omega}_\pi d\Omega_\tau} = \kappa_{\ell\gamma}\kappa_\rho \frac{\alpha^2\beta_\tau}{64E_\tau^2}(D_0 A' A + D_{ij} B_i B_j')W \tag{1.89}$$

In the c.m.s. the $\tau^{\mp}$ directions are limited on a arc (Φ_A, Φ_B). The neutrino mass constraint in the decay $\tau^+ \to \rho^+\nu$ is written as $(p_\tau - p_\rho)^2 = 0$, which gives the τ^+ production angle, Θ_τ, with respect the ρ direction $\vec{n}_\rho$. This relation says that the τ^+ direction $\vec{n}_\tau$, which lies on a unit sphere, is on the circumference of a circle C_ρ with radius equal to $\sin\Theta_\tau$, as shown in Fig. 1.9. Similarly the invariant mass $M_{\nu\bar{\nu}} > 0$ of the two neutrino system in the decay $\tau^- \to l^-\nu\bar{\nu}\gamma$ give a constraint to Θ_τ', where Θ_τ' is the τ angle along the

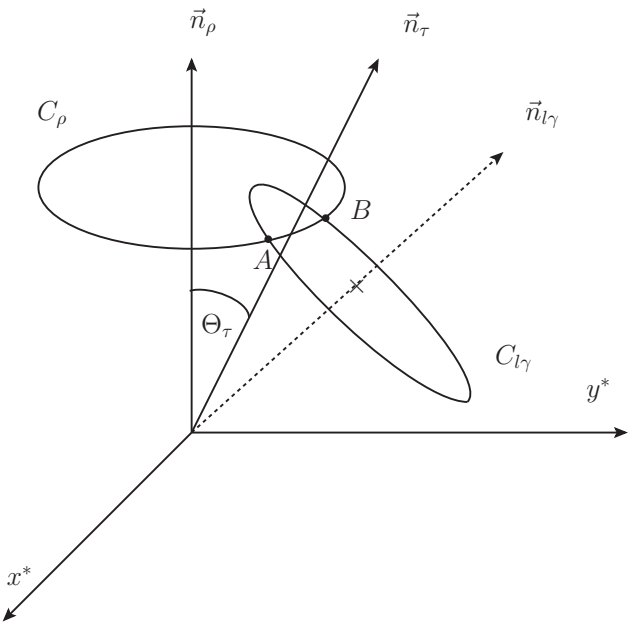

FIGURE 1.9: Configuration of the two circles C_ρ and $C_{l\gamma}$ on a unit sphere, which are determined from the decay $\tau^+ \to \rho^+\nu$ and $\tau^- \to l^-\nu\bar{\nu}\gamma$, respectively. The kinematically allowed region for C_ρ is the circumference and the region $C_{l\gamma}$ is either inside or outside of the circle, depending on $\cos\Theta_\tau > 0$ or < 0

direction of the $l\gamma$ system. The inequality $M_{\nu\bar{\nu}} > 0$ confines the vector $\vec{n}_\tau$ inside the circle $C_{l\gamma}$. Therefore, in the c.m.r., the direction of the $\tau^\mp$ system is given by the intersection between the circumference of C_ρ and the circle $C_{l\gamma}$, i.e. the arc (Φ_A, Φ_B).

Experimentally we measure particle parameters in the c.m.s., hence visible differential cross section is given by [128]:

$$\mathcal{F}(p_\ell, \Omega_\ell, p_\gamma, \Omega_\gamma, p_\rho, \Omega_\rho, m^2_{\pi\pi}, \tilde{\Omega}_\pi) = \frac{d\sigma(\ell^\mp\gamma, \rho^\pm)}{dp_\ell d\Omega_\ell dp_\gamma d\Omega_\gamma dp_\rho d\Omega_\rho dm^2_{\pi\pi} d\tilde{\Omega}_\pi} =$$
$$= \int_{\Phi_A}^{\Phi_B} \frac{d\sigma(\ell^\mp\gamma, \rho^\pm)}{dE^*_\ell d\Omega^*_\ell dE^*_\gamma d\Omega^*_\gamma d\Omega^*_\rho dm^2_{\pi\pi} d\tilde{\Omega}_\pi d\Omega_\tau} \left| \frac{\partial(E^*_\ell, \Omega^*_\ell, E^*_\gamma, \Omega^*_\gamma, \Omega^*_\rho, \Omega_\tau)}{\partial(p_\ell, \Omega_\ell, p_\gamma, \Omega_\gamma, p_\rho, \Omega_\rho, \Phi_\tau)} \right| d\Phi_\tau, \quad (1.90)$$

where the integration is done over the unknown tau direction, which is constrained by (Φ_A, Φ_B) arc. Both Φ_A and Φ_B angles are calculated using parameters measured in the experiment. The Jacobian in Eq.(1.90) can be further simplified as:

$$\left| \frac{\partial(E^*_\ell, \Omega^*_\ell, E^*_\gamma, \Omega^*_\gamma, \Omega^*_\rho, \Omega_\tau)}{\partial(p_\ell, \Omega_\ell, p_\gamma, \Omega_\gamma, p_\rho, \Omega_\rho, \Phi_\tau)} \right| = \left| \frac{\partial(E^*_\ell, \Omega^*_\ell)}{\partial(p_\ell, \Omega_\ell)} \right| \cdot \left| \frac{\partial(E^*_\gamma, \Omega^*_\gamma)}{\partial(p_\gamma, \Omega_\gamma)} \right| \cdot \left| \frac{\partial(\Omega^*_\rho, \Omega_\tau)}{\partial(p_\rho, \Omega_\rho, \Phi_\tau)} \right|, \quad (1.91)$$

where the expressions for the latter Jacobians can be found in [128].

In our feasibility study we developed special generator of the signal ($\ell^\mp\nu\nu\gamma$, $\pi^\pm\pi^0\nu$) events.

TABLE 1.7: Sensitivities to $\tilde{a}_\tau$ and $\tilde{d}_\tau$ in radiative leptonic decays of τ (ρ-tag and full tag cases), which can be achieved with the whole data sample collected at Belle and planned in Belle II experiment. Results of the previous most precision studies done at DELPHI and Belle are also shown in the last two strings.

	$\mathrm{Re}(\tilde{a}_\tau)$	$\mathrm{Im}(\tilde{a}_\tau)$	$\mathrm{Re}(\tilde{d}_\tau)$	$\mathrm{Im}(\tilde{d}_\tau)$
Belle (ρ-tag)	0.16	0.16	0.15	0.046
Belle-II (ρ-tag)	0.023	0.023	0.021	0.007
Belle (full tag)	0.085	0.085	0.080	0.024
Belle-II (full tag)	0.012	0.012	0.011	0.003
DELPHI	0.017	—	—	—
Belle	—	—	0.0015	0.0008

For the unbinned maximum likelihood fit of the generated events the PDF is constructed as ($\vec{X} = (p_\ell, \Omega_\ell, p_\gamma, \Omega_\gamma, p_\rho, \Omega_\rho, m^2_{\pi\pi}, \tilde{\Omega}_\pi)$):

$$\mathcal{P}(\vec{X}) = \frac{\mathcal{F}(\vec{X})}{\int \mathcal{F}(\vec{X}) d\vec{X}} \tag{1.92}$$

By fitting samples of generated events corresponding to the amount of data available at Belle [122–125] and expected at Belle II [61, 62] we studied sensitivities to $\tilde{a}_\tau$ and $\tilde{d}_\tau$ parameters.

Obtained results are collected in Table 1.7. The sensitivities are shown for two cases: events are tagged by $\tau^\pm \to \rho^\pm\nu$ only (ρ-tag); six decay modes with the total branching fraction of about 90% are used for the tag: $\tau^\pm \to \rho^\pm\nu$, $\tau^\pm \to \pi^\pm\nu$, $\tau^\pm \to \pi^\pm\pi^0\pi^0\nu$, $\tau^\pm \to \pi^\pm\pi^+\pi^-\nu$, $\tau^\pm \to e^\pm\nu\nu$, $\tau^\pm \to \mu^\pm\nu\nu$ (full tag). In the full-tag case, the sensitivity increase due to the statistical factor $\sqrt{90/25.5} = 1.88$ (comparing with ρ-tag case with Br=25.5%) We noted that the integration over (Φ_A, Φ_B) arc inflates the uncertainty by a factor of 1.4 (in comparison with the case when direction of tau is known). Also, inclusion of the spin dependent part of the differential decay width gives $\sim$ 1.5 increase in the sensitivity to $\tilde{a}_\tau$ and $\tilde{d}_\tau$. It is interesting to note that for events with $\tau \to e\nu\bar{\nu}\gamma$ the sensitivity is two times worse than for $\tau \to \mu\nu\bar{\nu}\gamma$ (for the same statistics). In Tab. 1.7 the sensitivities to $\tilde{a}_\tau$ and $\tilde{d}_\tau$ obtained in the previous most precise studies at DELPHI [16] and Belle [19] are also shown for the comparison. It is clearly seen that the measurement of $\mathrm{Re}(\tilde{a}_\tau)$ and $\mathrm{Im}(\tilde{a}_\tau)$ in τ radiative leptonic decays at Belle II with the full tag can be already competitive with DELPHI result. While the expected sensitivity to $\mathrm{Re}(\tilde{d}_\tau)$ and $\mathrm{Im}(\tilde{d}_\tau)$ is still worse than the most precise measurement of $\tilde{d}_\tau$ in $\tau^+\tau^-$ production vertex done at Belle.

Concerning our expectation on tau dipole moments $\mathcal{O}(10^{-3})$, it was difficult to estimate the

sensitivity in this multidimensional likelihood fit before performing it. Here the question was how strong are the peculiarities of the multidimensional shape associated with additional $\tilde{a}_\tau$ and $\tilde{d}_\tau$ terms. We can have better upper limits if the shapes are bigger enough. But even from the beginning it was clear that functions G_a, G_d, J_a etc., are suppressed in comparison with G, J, K: at small y-values $G \sim 1/y^2$ but $G_a \sim 1$ ($y = 2E_\gamma/m_\tau$). So the sensitivity is determined by interplay between peculiarities of dipole moments related shapes, which tend to increase the sensitivity, and the mentioned suppression, which tend to decrease it. Eventually, it could be solved only in the real feasibility study.

Chapter 2

Top Quark Dipole Moments

2.1 Introduction

In view of its large mass the top quark is a unique probe of the dynamics that breaks the electroweak gauge symmetry. While the observation of a Higgs boson at the CERN LHC [130, 131] and first measurements of its production and decay channels appear to be consistent with the Standard Model (SM) Higgs mechanism of electroweak symmetry breaking, this mechanism is still far from being validated at high precision. Deviations from the SM are likely to be most pronounced in processes involving top quarks. They may become manifest as deviations of the top-quark gauge-boson couplings from the values predicted by the SM (see [4, 5] for overviews).

Several studies have established photon radiation in top quark pair production at hadron colliders as potential probe of anomalous coupling effects [13], which could be improved upon only at a future high-energy electron-positron collider by exploiting final state correlations [14] in top quark pair production. The production of $t\bar{t}\gamma$ final states was first measured at the Tevatron [132], and studies at the LHC are ongoing [133, 134]. While indirect constraints on anomalous electromagnetic couplings from electroweak precision data or flavour physics observables turn out to be very constraining for bottom quarks [8–10], only loose constraints can be obtained in the case of top quarks (see [11, 12] for recent studies).

With the hadron collider cross sections for top quark pair production and single top quark production being of comparable magnitude, it appears worthwhile to extend the considerations made in [13] to photon radiation in single top quark production as probe of anomalous electromagnetic couplings of the top quark. It is the aim of the present chapter to investigate the sensitivity of photon radiation in single top quark production events on

anomalous electromagnetic couplings of the top quark. In Sec. 2.2, we give an overview of the photonic vertex function of the top quark, and the we will introduce its effective field theory expansion defining the top quark electric and magnetic dipole moments (Sec. 2.3). The parton-level phenomenology of these new operators will be discussed in Sec. 2.4, followed by numerical results for signal and background processes contributing to single-top-plus photon production in view of a determination of anomalous couplings in this process (Sec. 2.5). These results are used in Section 2.6 to quantify the sensitivity of future LHC data on these couplings.

2.2 SM prediction for top dipole moments

In this section we briefly analyze the current determination of the top quark dipole moments.

2.2.1 Top anomalous magnetic moment

The top form factor $F_{2V}(q^2)$, appearing in (1.1), can be computed in perturbation theory and they are known for heavy quarks to one loop in the electroweak theory [38, 135, 136] and two loops in QCD [137–139]. As already highlighted, in general the form factors are not physical quantities for any q^2, since they are gauge dependent and infrared divergent. However the quantities $F_{2V}(0)$ and $F_{2A}(0)$ have physical meaning: they can be defined as the residues of the photon pole in scattering amplitudes in the soft photon limit. Moreover they are gauge invariant (with respect to the full SM gauge group) and infrared-finite.

SM values for the static dipole moments can be derived from the form factors results. It is important to note that, compared to the case of leptons, heavy quarks anomalous magnetic moment receives the largest contribution from QCD corrections. QCD contributions to heavy quark $g-2$ are known up to three-loop level:

$$a_t^{\mathrm{QCD}} = \frac{\alpha_s}{2\pi} C_F + \left(\frac{\alpha_s}{2\pi}\right)^2 A_Q^{(2l)} + \left(\frac{\alpha_s}{2\pi}\right)^3 A_Q^{(3l)} + \mathcal{O}\left(\alpha_s^4\right), \tag{2.1}$$

where the QCD coupling $\alpha_s = \alpha_s(\mu)$, with μ the renormalization scale, is defined in the standard $\overline{\mathrm{MS}}$ scheme with N_l massless quarks and one quark Q with mass m_Q.

The leading contribution arises from the one-loop digram in Fig. 2.1 in which a virtual gluon is exchanged (instead of a virtual photon as in the case of a lepton). The mass independent result is [140]

$$a_q^{\mathrm{LO}} = \frac{\alpha_s}{2\pi} C_F, \tag{2.2}$$

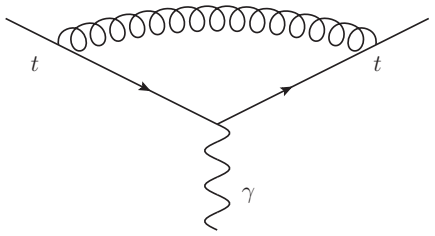

FIGURE 2.1: leadin contribution to the top anomalous magnetic moment.

in analogy with the leading contribution to the the electron $g-2$ $\alpha_{\rm em}/(2\pi)$ [25].

Two-loop contributions in QCD has the analytic compact form [140]:

$$\begin{aligned} A_Q^{(2l)} = & C_F^2\left(-\frac{32}{4}+2\zeta_2\left(5-6\ln(2)\right)+3\zeta_3\right) \\ & + C_F C_A\left(-\frac{317}{36}+3\zeta_2\left(-1+2\ln(2)\right)-\frac{3}{2}\zeta_3\right) \\ & + C_F T_F\left(\frac{119}{9}-8\zeta_2\right)-\frac{25}{9}C_F T_F N_l + C_F\beta_0\ln\left(r_Q\right), \end{aligned} \tag{2.3}$$

where $r_Q = \mu^2/m_Q^2$, ζ_n is the Reimann zeta function, and $C_F = (N_c^2-1)/2N_C$, $C_A = N_c$, $T_F = 1/2$ with $N_c = 3$ being the number of colors. Furthermore $\beta_0 = (11C_A - 4T_F(N_l + 1)/6)$. The analytic expression for the three-loop QCD coefficient $A_Q^{(3l)}$ was computed in [141] and it is not reported here.

Numerical results for the case of the bottom and top quark are reported in Tab. 2.1 where in the case $Q = t$, values are computed in $N_f = N_l + 1$ flavour QCD with $N_l = 5$, i.e. all quarks but the top taken to be massless, while for $Q = b$ it is assumed $m_i = 0$ $(i = u, d, s, c)$ and $m_b \neq 0$. Two-loop contribution to a_t and a_b are about 30 and 70 percent of the respective leading terms of order α_s. Also, three-loop corrections size are comparable to the two-loop ones. For the top quark they represent about 10 percent of the total anomalous moment, whereas for the bottom they give 30% correction.

As already anticipated, electroweak corrections are subleading with respect to the QCD one. The first QED contribution, similar to that one in Eq. (1.11), provides with the result:

$$a_Q^{\rm EW} = Q^2\frac{\alpha_{\rm e.m.}}{2\pi}, \tag{2.4}$$

where Q is the heavy quark charge and $\alpha_{\rm e.m.}$ is the fine structure constant. In the case of top quark, QED contribution is of $\mathcal{O}(10^{-3})$, i.e. of the same order of magnitude of the three loop QCD corrections.

In any case, the level of precision required by three-loop QCD corrections and the QED one is beyond the estimated achievable sensitivity of future hadron colliders and flavor

physics experiments.The best constraints on top anomalous couplings can at present be obtained from a combination of the direct production process $p\bar{p} \to t\bar{t}\gamma$ [**?**] and flavour observables. They read [12]:

$$\begin{aligned} -3.0 < \quad a_t \quad &< 0.45 \,, \\ -0.29 \times 10^{-16} e\,\mathrm{cm} < \quad d_t \quad &< 0.86 \times 10^{-16} e\,\mathrm{cm} \,. \end{aligned} \tag{2.5}$$

	$t \quad (\mu = m_t)$	$b \quad (\mu = m_b)$
$a_Q^{(1l)}$	$2.29 \cdot 10^{-2}$	$4.55 \cdot 10^{-2}$
$a_Q^{(2l)}$	$7.1 \cdot 10^{-3}$	$3.01 \cdot 10^{-2}$
$a_Q^{(3l)}$	$2.5 \cdot 10^{-3}$	$2.43 \cdot 10^{-2}$
a_Q	$3.25 \cdot 10^{-2}$	$7.56 \cdot 10^{-2}$

TABLE 2.1: One-, two- and three-loop contributions, and their sum, to the anomalous magnetic moments of the top and bottom quark. Input values are $m_t = 175$ GeV, $m_b = 5$ GeV, $\alpha_s(m_t) = 0.1080$, $\alpha_s(m_b) = 0.2145$ [140].

2.3 Effective field theory approach to top quark dipole moments

Following the approach described for the case of tau lepton, also discussed in [12, 142–144], we chose to describe dipole moments effects in top production via an effective Lagrangian

$$\mathcal{L}_{\text{eff}} = -\Delta a_t \frac{Q_t e}{4m_t} \bar{t}\sigma_{\mu\nu} t F^{\mu\nu} + i\frac{\Delta d_t}{2} \bar{t}\sigma_{\mu\nu}\gamma_5 t F^{\mu\nu}. \tag{2.6}$$

The couplings Δa_t and Δd_t are reals and related to the top quark $g-2$ and EDM.

We recall that the interacting Lagrangian (2.6) actually must be thought as arising within the framework of gauge-invariant effective operators, which results after integrating the heavy degrees of freedom associated to possible NP. The large number and variety of dimension-six operators [64] leads to the appearance of many possible Lorentz structures for the top trilinear vertices , involving a large number of parameters:

$$\mathcal{L}_{\text{eff}} = \sum_i \frac{C_i}{\Lambda^2} \mathcal{O}_i. \tag{2.7}$$

Some of these operators are redundant and can be eliminated through the equation of motion [142]. Therefore phenomenological studies can be carry on using simpler Lagrangian.

In the case of electromagnetic dipole moments interactions, as shown in [142, 145] there are two, and only two, dimension-six gauge-invariant operators that give rise to both the

$g-2$ and EDM,

$$\mathcal{O}_{uB\varphi}^{33} = C_{uB\varphi}^{33}\bar{q}_{L3}\sigma^{\mu\nu}t_R\tilde{\varphi}B_{\mu\nu} + \text{h.c.}\,,$$
$$\mathcal{O}_{uW}^{33} = C_{uW}^{33}\bar{q}_{L3}\sigma^{\mu\nu}\tau^a t_R\tilde{\varphi}W_{\mu\nu}^2 + \text{h.c.}\,, \tag{2.8}$$

where the new physics scale is $\Lambda \gg v$, and the coefficients $C_{uB\varphi}^{33}$ and C_{uW}^{33} are related to the parameters in (2.6) via

$$\Delta a_t \frac{Q_t}{4} = \frac{\sqrt{2}}{e}\text{Re}\left[c_W C_{uB\varphi}^{33} + s_W C_{uW}^{33}\right]\frac{vm_t}{\Lambda^2}, \tag{2.9}$$
$$\Delta d_t/2 = \frac{\sqrt{2}}{e}\text{Im}\left[c_W C_{uB\varphi}^{33} + s_W C_{uW}^{33}\right]\frac{v}{\Lambda^2}. \tag{2.10}$$

It is interesting to note that the vector coupling γ^μ in (1.1) does not receive corrections from the dimension-six operators. Redundant operators, like $\mathcal{O}_{qW}, \mathcal{O}_{qB}$ and $\mathcal{O}_{uB}$ of Ref. [64], would yield corrections $\sim q^2\bar{t}_L\gamma^\mu t_R$. A redefinition of such operators eliminates such terms [142], so that corrections to the electromagnetic coupling are absent. Additional q^2 terms in the form factors would arise from higher-dimensional operators (e.g. dimension-8 operators) and thus are further suppresses by power of q^2/Λ^2. For this reason in it is important to not have the momentum in the process above the Λ scale.

2.4 Top quark dipole moment in single-top-plus-photon production

The measurement of Δa_t and Δd_t is extremely challenging because of the very short mean life of the quark that makes it impossible to measure the two parameters by the interaction with an external electromagnetic field. Bounds on the anomalous couplings of the top can be inferred from the cross section for $t\bar{t}$ pair production and single-top production at the LHC. Their extraction in top quark pair production from $t\bar{t}\gamma$ and $t\bar{t}Z$ final states was investigated in detail in [13]. These measurements can be complemented by single-top quark production processes, which we study here.

Single top quark production at LHC is largely dominated by the t-channel process: $pp \to t + j$ with a light quark jet in the final state [146, 147]. A potential probe of anomalous couplings in the top quark sector thus proceeds through the reaction

$$pp \to tj\gamma. \tag{2.11}$$

To quantify the potential effect of an anomalous magnetic moment of the top quark on this process, we first consider the parton-level reaction

$$ub \to td\gamma, \tag{2.12}$$

at fixed centre-of-mass energy, and in the rest frame of the incoming partons.

Cross sections are obtained with a Fortran code generated by `FeynArts` and `FormCalc` [107, 148]. The new operators appearing in Eq. (1.43) are implemented in FeynArts with the Mathematica package `FeynRules` [149]. Following the above reasoning, we focus our discussion on the CP-conserving coupling $\Delta a_t \neq 0$ and set $\Delta d_t = 0$. The total cross section σ for the reaction in Eq. (2.12) can be split in three contributions,

$$\sigma = \sigma_{\rm SM} + \Delta a_t \sigma_a + \Delta a_t^2 \sigma_{aa}, \tag{2.13}$$

where $\sigma_{\rm SM}$ is the leading-order Standard Model prediction, the term σ_a linear in Δa_t arises from the interference between Standard Model and the anomalous amplitudes, whereas the quadratic term σ_{aa} is the self-interference of the anomalous amplitudes.

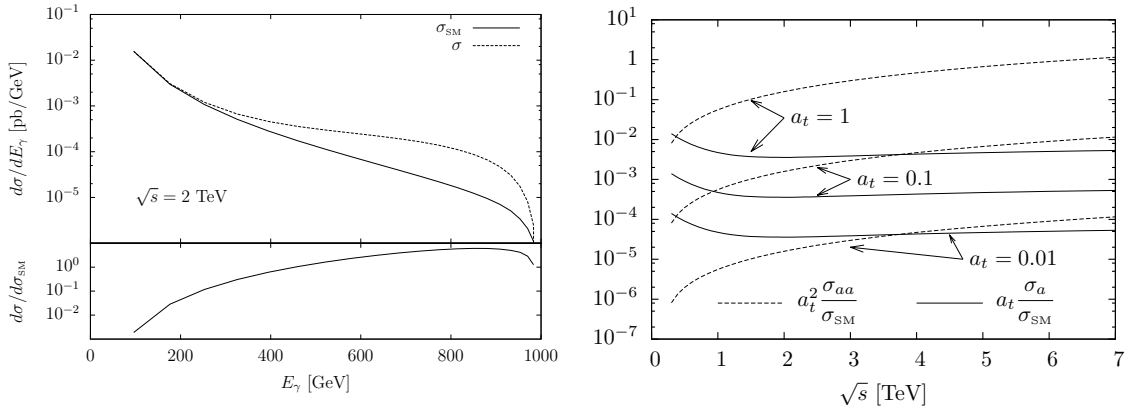

FIGURE 2.2: The parton-level cross section for $ub \to td\gamma$. Left: Photon energy distribution at $\sqrt{s} = 2$ TeV. Standard Model process and anomalous contribution for $\Delta a_t = 1$, $\Delta d_t = 0$. Right: The parton-level cross section as function of the parton-parton centre-of-mass energy $\sqrt{s}$. Ratio of the anomalous terms σ_a and σ_{aa} to the Standard Model process for different values of Δa_t.

We observe in Fig. 2.2 (left) that a contribution from the $g-2$ coupling gives a photon energy spectrum harder than the SM one because of the grow with $\sqrt{s}$ associated to the dimension 5 operators in Eq. (1.43). The relative importance of the linear and quadratic terms σ_a and σ_{aa} is illustrated in Fig. 2.2 (right). It can be seen that for large $|\Delta a_t| > 0.1$, the quadratic term σ_{aa} clearly dominates over the interference contribution σ_a. This feature can be understood from the helicity structure of the amplitudes for the Standard Model process and for the anomalous contribution. As a consequence, we expect a bound

on Δa_t to be almost insensitive on the sign and limited by quadratic dependence of the cross section on the anomalous coupling.

As already anticipated in the previous section, analogous results are obtained for a non-zero electric dipole moment case when the role of the dimensionless parameter Δa_t is played by $\Delta d_t(2m_t/Q_t e)$.

2.5 Numerical results for signal and background processes

To assess the potential of single-top-plus-photon production at the LHC (with centre-of-mass energy of 14 TeV), we concentrate on photon radiation in the t-channel single top production process, $pp \to tj\gamma$, followed by $t \to bW^+$, where the W boson decays into an electron or a muon (τ leptons are ignored). We take into account also t-channel single-top production followed by top radiative decay ($t \to bl\nu_l\gamma$). The process is combined with its charge conjugate $pp \to \bar{t}j\gamma$, followed by $\bar{t} \to \bar{b}W^-$. From now on we will refer to these processes simply as "single-top+γ". In the final state of the processes

$$\begin{aligned} pp &\to \gamma l^+ \nu_l b j, \\ pp &\to \gamma l^- \bar{\nu}_l \bar{b} j \quad \text{with } l = e, \mu, \end{aligned} \tag{2.14}$$

we require two jets, one of them tagged as a b-jet, a hard isolated photon, an isolated lepton and missing energy from the undetected neutrino.

We generate at leading-order parton-level event samples with `MadGraph5` [150]. Besides its Standard Model electromagnetic interaction, the top quark couples with the photon also via the effective operators introduced in Eq. (1.43), by means of a new Madgraph model generated with `FeynRules` [149]. We assume in general contributions from both the anomalous electric and magnetic dipole moments. In the simulation the top quark mass is $m_t = 173.5$ GeV and all other quarks and leptons masses are set to zero. The single-top cross section is computed in the five-flavour scheme and includes top quark and W decay width effects and full spin correlations. All cross sections for signal and background are computed using CTEQ6L1 parton distribution [151]. The renormalization and factorization scales are chosen event-by-event to be

$$\mu_F^2 = \mu_R^2 = m_t^2 + \sum_i p_T^2(i), \tag{2.15}$$

where m_t is the top mass and the index i runs over the visible particles in the final state.

The acceptance cuts for signal and background events are

$$\begin{gathered} p_T(\gamma) > 100 \text{ GeV}, \quad p_T(j) > 20 \text{ GeV}, \quad p_T(b) > 20 \text{ GeV}, \quad \not{p}_T > 20 \text{ GeV}, \\ |\eta(\gamma)| < 2.5, \quad |\eta(b)| < 2.5, \quad |\eta(j)| < 5, \quad |\eta(l)| < 2.5, \\ \Delta R(j,b) > 0.4, \quad \Delta R(j,l) > 0.4, \quad \Delta R(j,\gamma) > 0.4, \\ \Delta R(l,\gamma) > 0.4, \quad \Delta R(l,b) > 0.4, \quad \Delta R(b,\gamma) > 0.4, \end{gathered} \tag{2.16}$$

where $\Delta R^2 = \Delta\Phi^2 + \Delta\eta^2$ is the separation in the rapidity-azimuth plane and $\not{p}_T$ is the missing momentum due to the undetected neutrino.

The large cut on the photon transverse momentum enhances the contribution from the anomalous couplings, which grow with the photon energy. As a side effect, it also results in a suppression of Standard Model background processes yielding the same final state signature.

In addition to the cuts listed above, we also require the final state to be consistent with the single-top+γ production. In particular to reduce the background, the invariant mass $m(lb\nu)$ of the b-jet, the charged lepton and the neutrino should be close to the top mass. We choose to apply the technique in Ref. [152] for the reconstruction of the unmeasured z-component of the neutrino momentum $p_z(\nu)$. The transverse momentum of the neutrino is given by the x- and y-components of the $\not{E}_T$ vector, while the z-component $p_z(\nu)$ is inferred by imposing a W-boson mass constraint on the lepton-neutrino system. Since the constraint leads to a quadratic equation for $p_z(\nu)$, in case of two real solutions the smaller one $|p_z|$ is chosen. If the solutions are complex, the neutrino p_x and p_y are rescaled such that the imaginary radical vanishes, but keeps the transverse component of the neutrino as close as possible to $\not{E}_T$. In the end we select events with:

$$150 \text{ GeV} < m(lb\nu) < 200 \text{ GeV}. \tag{2.17}$$

The assumption $m(lb\nu) \sim m_t$ does not take into account the possibility of the radiative top decay where $m_t \sim m(lb\nu\gamma)$. However we checked that the contribution to the total cross section arising from radiative top decay is suppressed by the cut on the photon transverse momentum.

2.5.1 Signal cross section

Imposing the cuts listed in Eqs. (2.16) and (2.17) we obtain a cross sections for single-top-plus-photon production at the $\sqrt{s} = 14$ TeV LHC of 9.0 fb for final states involving a t

quark and 5.6 fb for final states involving a $\bar{t}$ quark. In the following, we will always add both these contributions to obtain the single-top-plus-photon production rates.

In Fig. 2.3 we show various distributions for single-top+γ production at the LHC. To illustrate the magnitude of potential effects, we compare the Standard Model prediction with a prediction including a non-standard $tt\gamma$ coupling with $a_t = 1.0$, $d_t = 0$. It can be seen that the photon spectrum is considerably harder in the high-p_T region when $a_t \neq 0$. Consequently, $g-2$ effects are enhanced in the configuration where the top quark (or its decay products b and l) are back to back to the photon, as shown in the ΔR distributions.

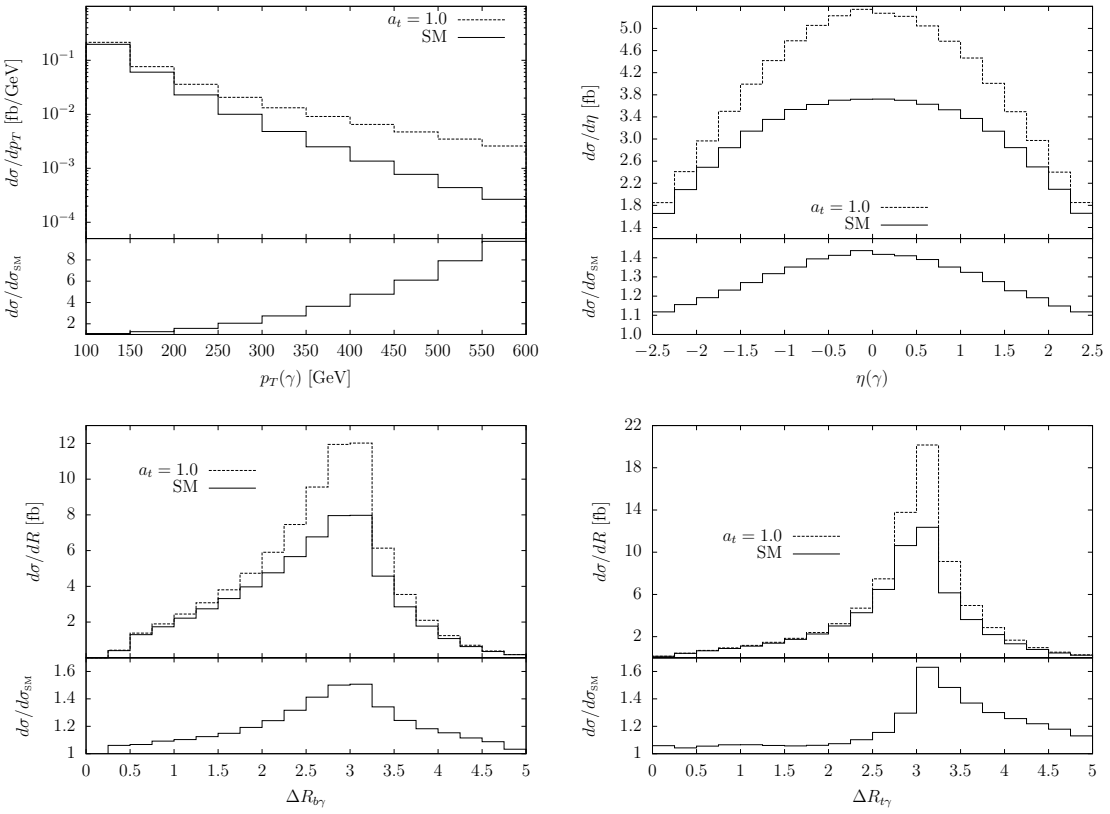

FIGURE 2.3: Kinematical distributions in single-top+γ production at the LHC with $\sqrt{s} = 14$ TeV.

2.5.2 Backgrounds

We distinguish two types of backgrounds: the irreducible background from the Standard Model process $pp \to (W \to l\nu_l)bj\gamma$, which yields the identical final state, and potentially reducible backgrounds from various other Standard Model processes that yield different

final states that are attributed to the single-top-plus-photon signature due to a misidentification of one or more of the final state objects.

The most important reducible background processes come from light jets faking either a b-jet or photon, or from electrons misidentified as a photons. In the analysis we assume a b-jet tagging efficiency of $\varepsilon_b = 60\%$ and a corresponding mistag rate of $\varepsilon_{\text{light}} = 0.1\%$ for a light jet (u, d, s quark or gluon) and $\varepsilon_c = 1\%$ for a c-jet, consistent with typical values assumed by the LHC experiments, e.g. [153] We apply the cuts in Eq. (2.16) where the (mistag) b-jet is chosen randomly.

A potentially dangerous background arises from jets misidentified as photons. To estimate the size of these processes we define a jet fake rate $f_{j\to\gamma}$ as the probability for a light jet to be misidentified as a photon. The rate $f_{j\to\gamma}$ is the one used in the experimental measurement of the $W\gamma$ and $Z\gamma$ cross section and the W+jet cross section at ATLAS [154], which estimated it to be $f_{j\to\gamma} \sim 1/2500$. Similar misidentification rates were reported in the expected performance for the ATLAS detector [155]. Background processes considered are $Wjjj$, $Wbjj$ and $Wbbj$ where a jet with at least $p_T > 100$ GeV fakes a photon (the $Wjjj$ process contributes only if it also yields a mistagged b-jet).

Electrons from W and Z boson decays can be misidentified as photons since the two particles generate similar electromagnetic signatures. The fake rate $f_{e\to\gamma}$, defined as the probability for a true electron to be identified as a converted photon, is estimated thorough the Z boson decay $Z \to ee$ as reported in the measurement of $W\gamma$, $Z\gamma$, $\gamma\gamma$ cross sections [154, 156]. The measured rate varies between 2% and 6% and in our case we conservatively assume $f_{e\to\gamma} \sim 6\%$. Since we require events with a certain amount of missing energy, the background taken into account here is the full leptonic $t\bar{t}$ production, where the two tops decay $t \to bl^+\nu_l$ and $\bar{t} \to \bar{b}e^-\bar{\nu}_e$. Processes involving a pair of vector bosons, such as $WWjj$ or $WZjj$, turn out to be irrelevant.

Other kinds of backgrounds result from Z-bosons decays to leptons, where one lepton is outside the detector coverage ($|\eta_l| > 2.5$) and fakes missing energy. Here we consider $Zbb\gamma$, $Zbj\gamma$, $Zjj\gamma$ and $t\bar{t}\gamma$. All these kinds of processes are negligible in our case.

Table 2.2 summarises the (Standard Model, without anomalous couplings) signal and background cross sections after the application of the cuts in Eqs. (2.16) and (2.17). For the single-top+γ cross section the b-tagging efficiency is included, thereby lowering the total cross section from the parton-level value stated above.

We observe that the signal process is two orders of magnitude larger than the irreducible background, and half the sum of all reducible background processes. It is clear that it will be possible to establish the Standard Model single-top-plus-photon process in the

Process	Measurable cross section [fb]
s single-top+γ	8.0
$Wbj\gamma$	$\mathcal{O}(10^{-2})$
$t\bar{t}$ full lep.	15.0
$W\gamma$+jets	1.5
W+jets	0.4
$t\bar{t}\gamma$	0.2
$Z\gamma$+jets	$\mathcal{O}(10^{-2})$
Z+jets	$\mathcal{O}(10^{-2})$

TABLE 2.2: Expected cross section for single-top+γ signal and the most important background processes at the LHC. Photon misidentification probabilities and b-jet mistag rates and efficiencies are included.

region of high photon-p_T already with moderate luminosity. However, a detection of anomalous couplings in this process requires a precision measurement of the cross section and of differential distributions. In the following, we use our simulation to determine the sensitivity of future LHC measurements of single-top-plus-photon process on a potential anomalous magnetic moment of the top quark.

2.6 Bounds from future LHC data

We use the shape of the photon transverse momentum distribution to derive quantitative sensitivity bounds that can be obtained on the anomalous dipole moments of the top quark. After imposing the cuts in Eqs. (2.16) and (2.17), we combine channels with electrons and muons in the final state. We perform a χ^2 test on the distributions and calculate 68.3% and 95% confidence level limits. The dominant backgrounds consist of $t\bar{t}$, $W\gamma$+jets and W+jets. Other sources of background are neglected. Limits at the LHC, with $\sqrt{s} = 14$ TeV are computed for an integrated luminosity of 30 fb^{-1} (one year of operation), 300 fb^{-1} (integrated luminosity expected from the upcoming run period) and 3000 fb^{-1} (high-luminosity upgrade option). The sensitivity bounds are shown in Fig. 2.4 and Tab. 2.3. As already discussed in Section 2.4 above, the measurement is insensitive on the sign of the anomalous dipole moments and on the interplay of Δa_t and Δd_t due to the dominance of the self-interference term.

Concentrating on the limits at 95% confidence level, we observe that with 30 fb^{-1} only contributions to the dipole moments at order unity could be detected. With higher luminosity, these limits improve towards 0.4 (at 300 fb^{-1}) and 0.2 (at 3000 fb^{-1}). Compared with the current bounds (2.5), which arise essentially from flavour physics observables and

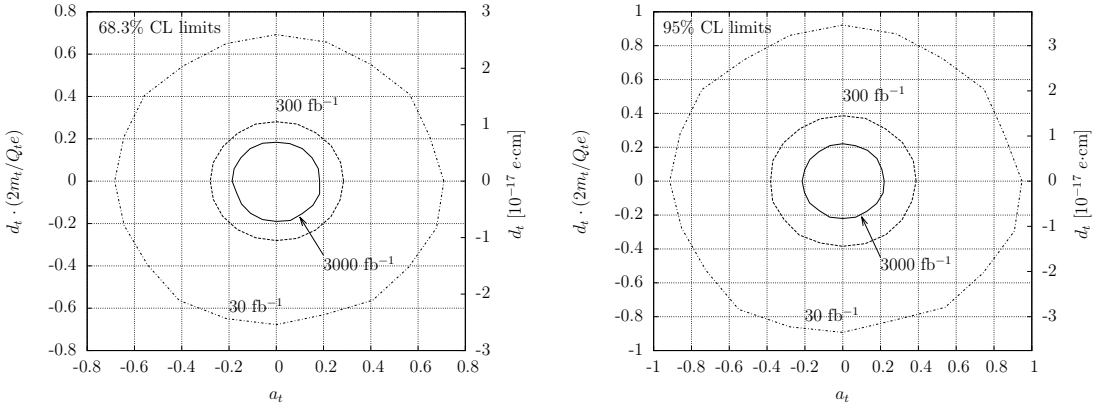

FIGURE 2.4: Bounds on the anomalous dipole moments of the top quark at 68% (left) and 95% (right) confidence level, for LHC operation at $\sqrt{s} = 14$ TeV.

coupling	30 fb^{-1}	300 fb^{-1}	3000 fb^{-1}
Δa_t	$^{+0.94}_{-0.92}$	$^{+0.39}_{-0.38}$	$^{+0.22}_{-0.21}$
Δd_t [$10^{-17} e$·cm]	$^{+3.5}_{-3.4}$	$^{+1.5}_{-1.5}$	$^{+0.83}_{-0.82}$

TABLE 2.3: Sensitivity achievable at 95% C.L. in single-top+γ at the LHC ($\sqrt{s} = 14$ TeV) for an integrated luminosities of 30 fb^{-1}, 300 fb^{-1} and 3000 fb^{-1}.

are thus of indirect nature, a significant improvement can be obtained. Depending on the sign of Δa_t or Δd_t, the improved constraints with a luminosity of 3000 fb^{-1} can be up to a factor 10 more restrictive than current bounds.

In [13], anticipated limits (for the same luminosity scenarios) from $t\bar{t}\gamma$ final states on the anomalous interactions of the top quarks were expressed in terms of the form factors $F_{2V}(0)$ and $F_{2A}(0)$ defined in Eq. (1.2). These limits can be converted in a straightforward manner into limits on the anomalous dipole moments considered here. The limits at 95% confidence level that are obtained by $t\bar{t}\gamma$ production are very similar to those obtained here from single-top-plus-photon production. Both channels are completely independent from each other, and a combination of them could thus further improve the sensitivity.

2.7 Conclusions

In this chapter, we have demonstrated the sensitivity of single-top-plus-photon production at the LHC on the anomalous dipole moments of the top quark. Contributions from the corresponding effective operators yield a photon transverse momentum spectrum that is harder than what is expected in the Standard Model. By simulating the signal process and all potentially relevant irreducible and reducible backgrounds to it, we have quantified the

numerical magnitude of anomalous top quark dipole moments that could be detected in the 14 TeV runs at the LHC with different luminosity scenarios. Our results are summarised in Figure 2.4, they demonstrate that the bounds that can be obtained from single-top-plus-photon production are very much comparable in magnitude to those that can be obtained from $t\bar{t}\gamma$ final states [13], and can potentially improve upon existing bounds [11, 12] by up to an order of magnitude.

Appendix A

Radiative leptonic decay: formulas.

The differential decay rate for $\tau \to \nu_\tau \bar{\nu}_\ell \ell \gamma$ is

$$\begin{aligned}\frac{d^6\,\Gamma}{dx\,dy\,d\Omega_\ell\,d\Omega_\gamma} &= \frac{\alpha\, m_\tau^5 G_F^2}{(4\pi)^8}\,\frac{xy\beta}{1+\delta_W(m_\mu,m_e)}\Big\{G(x,y,z)+x\beta\,\hat{n}\cdot\hat{p}_\ell\,J(x,y,z)\\ &\quad + y\,\hat{n}\cdot\hat{p}_\gamma\,K(x,y,z)+xy\beta\,\hat{p}_\ell\cdot(\hat{p}_\gamma\times\hat{n})\,L(x,y,z)\Big\}\,,\end{aligned} \tag{A.1}$$

with $r = m_\ell/m_\tau$, $\beta = \sqrt{1-4r^2/x^2}$ and $z = xy(1-c\,\beta)$. $\hat{n}$ is the unit vector in the direction of the τ's polarization.

$$\begin{aligned}G(x,y,z) &= G_{\rm LO}+\frac{\alpha}{\pi}\,G_{\rm NLO}+r_W^2 G_W+{\rm Re}(\tilde{a}_\tau)G_a+{\rm Im}(\tilde{d}_\tau)G_d\,,\\ J(x,y,z) &= J_{\rm LO}+\frac{\alpha}{\pi}\,J_{\rm NLO}+r_W^2 J_W+{\rm Re}(\tilde{a}_\tau)J_a+{\rm Im}(\tilde{d}_\tau)J_d\,,\\ K(x,y,z) &= K_{\rm LO}+\frac{\alpha}{\pi}\,K_{\rm NLO}+r_W^2 K_W+{\rm Re}(\tilde{a}_\tau)K_a+{\rm Im}(\tilde{d}_\tau)K_d\,,\\ L(x,y,z) &= {\rm Im}(\tilde{a}_\tau)L_a+{\rm Re}(\tilde{d}_\tau)L_d\,,\end{aligned} \tag{A.2}$$

with $r_W = m_\tau/M_W$. We neglect higher orders of α, r_W and $c_{a,d}$. The various functions generated by one of the effective operators take the following form:

$$G_{\rm LO} = -\frac{64\pi^2}{3y^2z^2}\left[\, r^4\left(6xy^2+6y^3-6y^2z-8y^2\right) + r^2\left(-4x^2y^2-6x^2yz-8xy^3+2xy^2z\right.\right.$$
$$+6xy^2+6xyz^2+8xyz+6xz^2-4y^4+5y^3z+6y^3-2y^2z^2-6y^2z-3yz^3+6yz^2$$
$$\left.-6z^3-8z^2\right)+4x^3yz+8x^2y^2z-8x^2yz^2-6x^2yz-4x^2z^2+6xy^3z-8xy^2z^2-6xy^2z$$
$$+6xyz^3-2xyz^2+8xz^3+6xz^2+2y^4z-2y^3z^2-3y^3z+2y^2z^3-2y^2z^2-2yz^4$$
$$\left.+5yz^3+6yz^2-4z^4-6z^3\right] \tag{A.3}$$

$$J_{\rm LO} = -\frac{64\pi^2}{3y^2z^2}\left\{6r^4y^2+r^2\left[y^2(-4x+z+2)+3yz(z-2x)-4y^3+6z^2\right]\right.$$
$$\left.+z\left[4x^2y+x\left(6y^2-2y(3z+1)-4z\right)+2y^3-y^2(4z+1)+yz(2z-3)+2z(2z+1)\right]\right\} \tag{A.4}$$

$$K_{\rm LO} = -\frac{64\pi^2}{3y^2z^2}\left\{6r^4y(y-z)+r^2\left[y^2(-4x+5z+2)+yz(x-2(z+1))+3z^2(x-z)-4y^3\right]\right.$$
$$-z\left[-2x^2(y-z)+x\left(-4y^2+4yz+y-z(4z+1)\right)-2y^3+y^2(2z+1)\right.$$
$$\left.\left.-2y(z-1)z+z^2(2z+1)\right]\right\} \tag{A.5}$$

$$G_a = \frac{64\pi^2}{3yz}\left\{r^2\left(y^2-zy+3z^2\right)-(x+y-z-1)z(y+2z)\right\}, \tag{A.6}$$

$$G_d = -\frac{128\pi^2}{3y^2z}\left\{6y^2r^4+\left(-3y^3+(-4x+z+2)y^2+3z(z-2x)y+6z^2\right)r^2\right.$$
$$+z\left(y^3-(3z+1)y^2+4x^2y+2(z-1)zy+2z(2z+1)\right.$$
$$\left.\left.+x\left(5y^2-2(3z+1)y-4z\right)\right)\right\}, \tag{A.7}$$

$$J_a = -\frac{64\pi^2}{3yz}\left\{-2y^3+\left(3r^2+2z+2\right)y^2-2x^2y+3zy-2z\left(3r^2+2z+1\right)\right.$$
$$\left.+x\left(3yr^2-4y^2+y+2yz+4z\right)\right\}, \tag{A.8}$$

$$J_d = \frac{128\pi^2}{3z}\left\{(-3x-3y+4)r^2+2x^2+2y^2-2y+x(4y-2z-3)-2yz+z\right\}, [1.5ex] \tag{A.9}$$

$$K_a = \frac{64\pi^2}{3y^2z}\Big\{ -12yr^4 + \left(3(x+2)y^2 + \left(3x^2+8x-8z-4\right)y - 6z^2\right)r^2 - 2x^3y + x^2y(-4y+2z+1) - 2z\left(-y^2-zy+y+2z^2+z\right) + x\left(-2y^3+2(z+1)y^2 + zy + 4z^2\right)\Big\}, \tag{A.10}$$

$$K_d = \frac{128\pi^2}{3y^2z}\Big\{ -2yx^3 + \left(-4y^2+(2z+3)y+4z\right)x^2 + \left(-2y^3+2(z+1)y^2+5zy - 2z(4z+3)\right)x + r^2\left(3yx^2+3y^2x-4yx-6zx+2y^2+6z^2-8yz+8z\right) + 2z\left(y^2-(3z+1)y+z(2z+3)\right)\Big\}, [1.5ex] \tag{A.11}$$

$$L_a = -\frac{32\pi^2}{3yz}\Big\{(-3x-3y+4)r^2 + 2x^2 + 2y^2 - 2y + x(4y-2z-3) - 2yz + z\Big\}, \tag{A.12}$$

$$L_d = \frac{64\pi^2}{3y^2z}\Big\{2y^3 - \left(3r^2+2z+2\right)y^2 + 2x^2y - 3zy + 2z\left(3r^2+2z+1\right) + x\left(4y^2 - \left(3r^2+2z+1\right)y - 4z\right)\Big\}. \tag{A.13}$$

Bibliography

[1] D. Hanneke, S. Fogwell, and G. Gabrielse, "New Measurement of the Electron Magnetic Moment and the Fine Structure Constant," Phys.Rev.Lett. **100**, 120801 (2008), 0801.1134.

[2] G. Bennett et al. (Muon G-2 Collaboration), "Final Report of the Muon E821 Anomalous Magnetic Moment Measurement at BNL," Phys.Rev. **D73**, 072003 (2006), hep-ex/0602035.

[3] G. Giudice, P. Paradisi, and M. Passera, "Testing new physics with the electron g-2," JHEP **1211**, 113 (2012), 1208.6583.

[4] H. Murayama and M. E. Peskin, "Physics opportunities of e+ e- linear colliders," Ann.Rev.Nucl.Part.Sci. **46**, 533 (1996), hep-ex/9606003.

[5] C. T. Hill and E. H. Simmons, "Strong dynamics and electroweak symmetry breaking," Phys.Rept. **381**, 235 (2003), hep-ph/0203079.

[6] M. Pospelov and A. Ritz, "Probing CP violation with electric dipole moments," (2010).

[7] L. Mercolli and C. Smith, "EDM constraints on flavored CP-violating phases," Nucl.Phys. **B817**, 1 (2009), 0902.1949.

[8] G. Altarelli, R. Barbieri, and S. Jadach, "Toward a model independent analysis of electroweak data," Nucl.Phys. **B369**, 3 (1992).

[9] G. Altarelli, R. Barbieri, and F. Caravaglios, "Nonstandard analysis of electroweak precision data," Nucl.Phys. **B405**, 3 (1993).

[10] O. J. Eboli, M. Gonzalez-Garcia, and S. Novaes, "Limits on anomalous top couplings from Z pole physics," Phys.Lett. **B415**, 75 (1997), hep-ph/9704400.

[11] J. F. Kamenik, M. Papucci, and A. Weiler, "Constraining the dipole moments of the top quark," Phys.Rev. **D85**, 071501 (2012), 1107.3143.

[12] A. O. Bouzas and F. Larios, "Electromagnetic dipole moments of the Top quark," Phys.Rev. **D87**, 074015 (2013), 1212.6575.

[13] U. Baur, A. Juste, L. Orr, and D. Rainwater, "Probing electroweak top quark couplings at hadron colliders," Phys.Rev. **D71**, 054013 (2005), hep-ph/0412021.

[14] B. Grzadkowski and Z. Hioki, "Optimal observable analysis of the angular and energy distributions for top quark decay products at polarized linear colliders," Nucl.Phys. **B585**, 3 (2000), hep-ph/0004223.

[15] J. Bernabeu, G. Gonzalez-Sprinberg, J. Papavassiliou, and J. Vidal, "Tau anomalous magnetic moment form-factor at super B/flavor factories," Nucl.Phys. **B790**, 160 (2008), 0707.2496.

[16] J. Abdallah et al. (DELPHI Collaboration), "Study of tau-pair production in photon-photon collisions at LEP and limits on the anomalous electromagnetic moments of the tau lepton," Eur.Phys.J. **C35**, 159 (2004), hep-ex/0406010.

[17] S. Eidelman and M. Passera, "Theory of the tau lepton anomalous magnetic moment," Mod.Phys.Lett. **A22**, 159 (2007), hep-ph/0701260.

[18] S. Berman and A. Sirlin, "Some considerations on the radiative corrections to muon and neutron decay," Ann.Phys. **20**, 20 (1962).

[19] K. Inami et al. (Belle Collaboration), "Search for the electric dipole moment of the tau lepton," Phys.Lett. **B551**, 16 (2003), hep-ex/0210066.

[20] A. Czarnecki and W. J. Marciano, "Electromagnetic dipole moments and new physics," (2010).

[21] B. L. Roberts and W. J. Marciano, "Lepton dipole moments," (2010).

[22] P. J. Mohr and B. N. Taylor, "CODATA recommended values of the fundamental physical constants: 2002," Rev.Mod.Phys. **77**, 1 (2005).

[23] K. Hagiwara et al. (Particle Data Group), "Review of particle physics. Particle Data Group," Phys.Rev. **D66**, 010001 (2002).

[24] T. Kinoshita and W. J. Marciano, *Quantum Electrodynamics* (World Scientific, 1990).

[25] J. S. Schwinger, "On Quantum electrodynamics and the magnetic moment of the electron," Phys.Rev. **73**, 416 (1948).

[26] C. M. Sommerfield, "Magnetic Dipole Moment of the Electron," Phys.Rev. **107**, 328 (1957).

[27] H. Elend, "On the anomalous magnetic moment of the muon," Physics Letters **20**, 682 (1966).

[28] M. Passera, "The Standard model prediction of the muon anomalous magnetic moment," J.Phys. **G31**, R75 (2005), hep-ph/0411168.

[29] M. Passera, "Precise mass-dependent QED contributions to leptonic g-2 at order alpha**2 and alpha**3," Phys.Rev. **D75**, 013002 (2007), hep-ph/0606174.

[30] S. Laporta and E. Remiddi, "The Analytical value of the electron (g-2) at order alpha**3 in QED," Phys.Lett. **B379**, 283 (1996), hep-ph/9602417.

[31] K. Nakamura et al. (Particle Data Group), "Review of particle physics," J.Phys. **G37**, 075021 (2010).

[32] R. Jackiw and S. Weinberg, "Weak interaction corrections to the muon magnetic moment and to muonic atom energy levels," Phys.Rev. **D5**, 2396 (1972).

[33] I. Bars and M. Yoshimura, "Muon magnetic moment in a finite theory of weak and electromagnetic interaction," Phys.Rev. **D6**, 374 (1972).

[34] G. Altarelli, N. Cabibbo, and L. Maiani, "The Drell-Hearn sum rule and the lepton magnetic moment in the Weinberg model of weak and electromagnetic interactions," Phys.Lett. **B40**, 415 (1972).

[35] W. A. Bardeen, R. Gastmans, and B. Lautrup, "Static quantities in Weinberg's model of weak and electromagnetic interactions," Nucl.Phys. **B46**, 319 (1972).

[36] K. Fujikawa, B. Lee, and A. Sanda, "Generalized Renormalizable Gauge Formulation of Spontaneously Broken Gauge Theories," Phys.Rev. **D6**, 2923 (1972).

[37] A. Czarnecki, B. Krause, and W. J. Marciano, "Electroweak Fermion loop contributions to the muon anomalous magnetic moment," Phys.Rev. **D52**, 2619 (1995), hep-ph/9506256.

[38] A. Czarnecki, B. Krause, and W. J. Marciano, "Electroweak corrections to the muon anomalous magnetic moment," Phys.Rev.Lett. **76**, 3267 (1996), hep-ph/9512369.

[39] G. Degrassi and G. Giudice, "QED logarithms in the electroweak corrections to the muon anomalous magnetic moment," Phys.Rev. **D58**, 053007 (1998), hep-ph/9803384.

[40] L. Bouchait and L. Michel, "La résonance dans la diffusion méson pi- méson pi et le moment magnétique anormal du méson mu," J. Phys. Radium (1961).

[41] L. Durand, "Pionic Contributions to the Magnetic Moment of the Muon," Phys.Rev. **128**, 441 (1962).

[42] S. J. Brodsky and E. De Rafael, "SUGGESTED BOSON - LEPTON PAIR COUPLINGS AND THE ANOMALOUS MAGNETIC MOMENT OF THE MUON," Phys.Rev. **168**, 1620 (1968).

[43] M. Gourdin and E. De Rafael, "Hadronic contributions to the muon g-factor," Nucl.Phys. **B10**, 667 (1969).

[44] B. Krause, "Higher order hadronic contributions to the anomalous magnetic moment of leptons," Phys.Lett. **B390**, 392 (1997), hep-ph/9607259.

[45] C. Jarlskog, "A Basis Independent Formulation of the Connection Between Quark Mass Matrices, CP Violation and Experiment," Z.Phys. **C29**, 491 (1985).

[46] C. Jarlskog, "Commutator of the Quark Mass Matrices in the Standard Electroweak Model and a Measure of Maximal CP Violation," Phys.Rev.Lett. **55**, 1039 (1985).

[47] L.-L. Chau and W.-Y. Keung, "Comments on the Parametrization of the Kobayashi-Maskawa Matrix," Phys.Rev.Lett. **53**, 1802 (1984).

[48] M. Kobayashi and T. Maskawa, "CP Violation in the Renormalizable Theory of Weak Interaction," Prog.Theor.Phys. **49**, 652 (1973).

[49] F. Hoogeveen, "The Standard Model Prediction for the Electric Dipole Moment of the Electron," Nucl.Phys. **B341**, 322 (1990).

[50] M. Pospelov and I. Khriplovich, "Electric dipole moment of the W boson and the electron in the Kobayashi-Maskawa model," Sov.J.Nucl.Phys. **53**, 638 (1991).

[51] E. Commins, "Electric dipole moments of leptons," Adv.At.Mol.Opt.Phys. **40**, 1 (1999).

[52] W. Bernreuther, O. Nachtmann, and P. Overmann, "The CP violating electric and weak dipole moments of the tau lepton from threshold to 500-GeV," Phys.Rev. **D48**, 78 (1993).

[53] F. Cornet and J. I. Illana, "Tau pair production via photon-photon collisions at LEP," Phys.Rev. **D53**, 1181 (1996), hep-ph/9503466.

[54] G. A. Gonzalez-Sprinberg, A. Santamaria, and J. Vidal, "Model independent bounds on the tau lepton electromagnetic and weak magnetic moments," Nucl.Phys. **B582**, 3 (2000), hep-ph/0002203.

[55] M. A. Samuel and G. Li, "Measuring the magnetic moment of the tau lepton at the Fermilab tevatron, the, SSC and the LHC," Int.J.Theor.Phys. **33**, 1471 (1994).

[56] F. del Aguila, F. Cornet, and J. I. Illana, "The Possibility of using a large heavy ion collider for measuring the electromagnetic properties of the tau-lepton," Phys.Lett. **B271**, 256 (1991).

[57] I. J. Kim, "Magnetic Moment Measurement of Baryons With Heavy Flavored Quarks by Planar Channeling Through Bent Crystal," Nucl.Phys. **B229**, 251 (1983).

[58] D. Chen et al. (E761 Collaboration), "First observation of magnetic moment precession of channeled particles in bent crystals," Phys.Rev.Lett. **69**, 3286 (1992).

[59] M. A. Samuel, G.-w. Li, and R. Mendel, "The Anomalous magnetic moment of the tau lepton," Phys.Rev.Lett. **67**, 668 (1991).

[60] K. Ikado et al. (Belle Collaboration), "Evidence of the Purely Leptonic Decay B -¿ tau- anti-nu(tau)," Phys.Rev.Lett. **97**, 251802 (2006), hep-ex/0604018.

[61] T. Aushev, W. Bartel, A. Bondar, J. Brodzicka, T. Browder, et al., "Physics at Super B Factory," (2010), 1002.5012.

[62] T. Abe et al. (Belle-II Collaboration), "Belle II Technical Design Report," (2010), 1011.0352.

[63] M. Laursen, M. A. Samuel, and A. Sen, "Radiation Zeros and a Test for the g Value of the τ Lepton," Phys.Rev. **D29**, 2652 (1984).

[64] W. Buchmuller and D. Wyler, "Effective Lagrangian Analysis of New Interactions and Flavor Conservation," Nucl.Phys. **B268**, 621 (1986).

[65] C. N. Leung, S. Love, and S. Rao, "Low-Energy Manifestations of a New Interaction Scale: Operator Analysis," Z.Phys. **C31**, 433 (1986).

[66] M. S. Bilenky and A. Santamaria, "One loop effective Lagrangian for a standard model with a heavy charged scalar singlet," Nucl.Phys. **B420**, 47 (1994), hep-ph/9310302.

[67] G. A. Gonzalez-Sprinberg, A. Santamaria, and J. Vidal, "Bounds on the tau magnetic moments: Standard model and beyond," Nucl.Phys.Proc.Suppl. **98**, 133 (2001), hep-ph/0103085.

[68] A. Ferroglia, C. Greub, A. Sirlin, and Z. Zhang, "Contributions of the W-boson propagator to muon and tau leptonic decay rates," Phys.Rev. **D88**, 033012 (2013), 1307.6900.

[69] A. Sirlin, "Radiative Corrections in the SU(2)-L x U(1) Theory: A Simple Renormalization Framework," Phys.Rev. **D22**, 971 (1980).

[70] R. Behrends, R. Finkelstein, and A. Sirlin, "Radiative corrections to decay processes," Phys.Rev. **101**, 866 (1956).

[71] S. Berman, "Radiative corrections to muon and neutron decay," Phys.Rev. **112**, 267 (1958).

[72] T. Kinoshita and A. Sirlin, "Radiative corrections to Fermi interactions," Phys.Rev. **113**, 1652 (1959).

[73] M. Roos and A. Sirlin, "Remarks on the radiative corrections of order alpha-squared to muon decay and the determination of g(mu)," Nucl.Phys. **B29**, 296 (1971).

[74] T. van Ritbergen and R. G. Stuart, "On the precise determination of the Fermi coupling constant from the muon lifetime," Nucl.Phys. **B564**, 343 (2000), hep-ph/9904240.

[75] T. van Ritbergen and R. G. Stuart, "Complete two loop quantum electrodynamic contributions to the muon lifetime in the Fermi model," Phys.Rev.Lett. **82**, 488 (1999), hep-ph/9808283.

[76] T. van Ritbergen and R. G. Stuart, "Hadronic contributions to the muon lifetime," Phys.Lett. **B437**, 201 (1998), hep-ph/9802341.

[77] M. Steinhauser and T. Seidensticker, "Second order corrections to the muon lifetime and the semileptonic B decay," Phys.Lett. **B467**, 271 (1999), hep-ph/9909436.

[78] A. Pak and A. Czarnecki, "Mass effects in muon and semileptonic b -¿ c decays," Phys.Rev.Lett. **100**, 241807 (2008), 0803.0960.

[79] A. Ferroglia, G. Ossola, and A. Sirlin, "Considerations concerning the radiative corrections to muon decay in the Fermi and standard theories," Nucl.Phys. **B560**, 23 (1999), hep-ph/9905442.

[80] T. Lee and C.-N. Yang, "Possible Nonlocal Effects in μ Decay," Phys.Rev. **108**, 1611 (1957).

[81] S. Eckstein and R. Pratt, "Radiative muon decay," Ann.Phys. **8**, 297 (1959).

[82] Q. Ho-Kim and X.-Y. Pham, "Elementary particles and their interactions," (1998).

[83] M. Krawczyk and D. Temes, "2HDM(II) radiative corrections in leptonic tau decays," Eur.Phys.J. **C44**, 435 (2005), hep-ph/0410248.

[84] D. Asner, T. Barnes, J. Bian, I. Bigi, N. Brambilla, et al., "Physics at BES-III," Int.J.Mod.Phys. **A24**, S1 (2009), 0809.1869.

[85] J. Beringer et al. (Particle Data Group), "Review of Particle Physics (RPP)," Phys.Rev. **D86**, 010001 (2012).

[86] A. Sirlin and A. Ferroglia, "Radiative Corrections in Precision Electroweak Physics: a Historical Perspective," Rev.Mod.Phys. **85**, 263 (2013), 1210.5296.

[87] W. Marciano and A. Sirlin, "Electroweak Radiative Corrections to tau Decay," Phys.Rev.Lett. **61**, 1815 (1988).

[88] S. Actis et al. (Working Group on Radiative Corrections and Monte Carlo Generators for Low Energies), "Quest for precision in hadronic cross sections at low energy: Monte Carlo tools vs. experimental data," Eur.Phys.J. **C66**, 585 (2010), 0912.0749.

[89] T. Kinoshita and A. Sirlin, "Muon Decay with Parity Nonconserving Interactions and Radiative Corrections in the Two-Component Theory," Phys.Rev. **107**, 593 (1957).

[90] A. Arbuzov, "First order radiative corrections to polarized muon decay spectrum," Phys.Lett. **B524**, 99 (2002), hep-ph/0110047.

[91] A. Arbuzov, A. Czarnecki, and A. Gaponenko, "Muon decay spectrum: Leading logarithmic approximation," Phys.Rev. **D65**, 113006 (2002), hep-ph/0202102.

[92] A. Arbuzov and K. Melnikov, "O(alpha**2 ln(m(mu) / m(e)) corrections to electron energy spectrum in muon decay," Phys.Rev. **D66**, 093003 (2002), hep-ph/0205172.

[93] A. Arbuzov, "Higher order QED corrections to muon decay spectrum," JHEP **0303**, 063 (2003), hep-ph/0206036.

[94] C. Anastasiou, K. Melnikov, and F. Petriello, "The Electron energy spectrum in muon decay through O(alpha**2)," JHEP **0709**, 014 (2007), hep-ph/0505069.

[95] A. I. Davydychev, K. Schilcher, and H. Spiesberger, "Hadronic corrections at O(alpha**2) to the energy spectrum of muon decay," Eur.Phys.J. **C19**, 99 (2001), hep-ph/0011221.

[96] M. Fischer, S. Groote, J. Korner, and M. Mauser, "Leptonic mu and tau decays: Mass effects, polarization effects and O(alpha) radiative corrections," Phys.Rev. **D67**, 113008 (2003), hep-ph/0203048.

[97] T. Aoyama, M. Hayakawa, T. Kinoshita, and M. Nio, "Tenth-Order QED Contribution to the Electron g-2 and an Improved Value of the Fine Structure Constant," Phys.Rev.Lett. **109**, 111807 (2012), 1205.5368.

[98] D. Webber et al. (MuLan Collaboration), "Measurement of the Positive Muon Lifetime and Determination of the Fermi Constant to Part-per-Million Precision," Phys.Rev.Lett. **106**, 041803 (2011), 1010.0991.

[99] C. Fronsdal and H. Uberall, "mu-Meson Decay with Inner Bremsstrahlung," Phys.Rev. **113**, 654 (1959).

[100] Y. Kuno and Y. Okada, "Muon decay and physics beyond the standard model," Rev.Mod.Phys. **73**, 151 (2001), hep-ph/9909265.

[101] A. Fischer, T. Kurosu, and F. Savatier, "QED one loop correction to radiative muon decay," Phys.Rev. **D49**, 3426 (1994).

[102] A. Arbuzov and E. Scherbakova, "One loop corrections to radiative muon decay," Phys.Lett. **B597**, 285 (2004), hep-ph/0404094.

[103] G. Passarino and M. Veltman, "One Loop Corrections for e+ e- Annihilation Into mu+ mu- in the Weinberg Model," Nucl.Phys. **B160**, 151 (1979).

[104] R. Mertig, M. Bohm, and A. Denner, "FEYN CALC: Computer algebraic calculation of Feynman amplitudes," Comput.Phys.Commun. **64**, 345 (1991).

[105] J. Vermaseren, "New features of FORM," (2000), math-ph/0010025.

[106] G. 't Hooft and M. Veltman, "Scalar One Loop Integrals," Nucl.Phys. **B153**, 365 (1979).

[107] T. Hahn and M. Perez-Victoria, "Automatized one loop calculations in four-dimensions and D-dimensions," Comput.Phys.Commun. **118**, 153 (1999), hep-ph/9807565.

[108] R. K. Ellis and G. Zanderighi, "Scalar one-loop integrals for QCD," JHEP **0802**, 002 (2008), 0712.1851.

[109] I. Mohammad and A. Donnachie, "Higher Order Corrections to Radiative Muon Decay in the Weinberg-Salam Model," (1976).

[110] P. Breitenlohner and D. Maison, "Dimensional Renormalization and the Action Principle," Commun.Math.Phys. **52**, 11 (1977).

[111] T. Kinoshita and A. Sirlin, "Radiative Decay of the Muon," Phys. Rev. Lett. **2**, 177 (1959), URL http://link.aps.org/doi/10.1103/PhysRevLett.2.177.

[112] T. Kinoshita, "Mass singularities of Feynman amplitudes," J.Math.Phys. **3**, 650 (1962).

[113] T. Lee and M. Nauenberg, "Degenerate Systems and Mass Singularities," Phys.Rev. **133**, B1549 (1964).

[114] R. Crittenden, W. Walker, and J. Ballam, "Radiative decay modes of the muon," Phys.Rev. **121**, 1823 (1961).

[115] T. Bergfeld et al. (CLEO Collaboration), "Observation of radiative leptonic decay of the tau lepton," Phys.Rev.Lett. **84**, 830 (2000), hep-ex/9909050.

[116] T. Hahn, "CUBA: A Library for multidimensional numerical integration," Comput.Phys.Commun. **168**, 78 (2005), hep-ph/0404043.

[117] J. Adam et al. (MEG Collaboration), "Measurement of polarized muon radiative decay," (2013), 1312.3217.

[118] S. Jadach, B. Ward, and Z. Was, "The Precision Monte Carlo event generator K K for two fermion final states in e+ e- collisions," Comput.Phys.Commun. **130**, 260 (2000), hep-ph/9912214.

[119] S. Jadach, Z. Was, R. Decker, and J. H. Kuhn, "The tau decay library TAUOLA: Version 2.4," Comput.Phys.Commun. **76**, 361 (1993).

[120] E. Barberio and Z. Was, "PHOTOS: A Universal Monte Carlo for QED radiative corrections. Version 2.0," Comput.Phys.Commun. **79**, 291 (1994).

[121] R. B. *et al.*, "GEANT 3.21," CERN Report No. DD/EE/84-1 (1984).

[122] A. Abashian, K. Gotow, N. Morgan, L. Piilonen, S. Schrenk, et al., "The Belle Detector," Nucl.Instrum.Meth. **A479**, 117 (2002).

[123] J. Brodzicka et al. (Belle Collaboration), "Physics Achievements from the Belle Experiment," PTEP **2012**, 04D001 (2012), 1212.5342.

[124] K. Akai, N. Akasaka, A. Enomoto, J. Flanagan, H. Fukuma, et al., "Commissioning of KEKB," Nucl.Instrum.Meth. **A499**, 191 (2003).

[125] T. Abe, K. Akai, N. Akasaka, M. Akemoto, A. Akiyama, et al., "Achievements of KEKB," PTEP **2013**, 03A001 (2013).

[126] Y.-S. Tsai, "Decay Correlations of Heavy Leptons in e+ e- —¿ Lepton+ Lepton-," Phys.Rev. **D4**, 2821 (1971).

[127] W. Fetscher, "Leptonic tau decays: How to determine the Lorentz structure of the charged leptonic weak interaction by experiment," Phys.Rev. **D42**, 1544 (1990).

[128] K. Tamai, "Correlated decay rates of a tau pair for the Michel parameter measurement," Nucl.Phys. **B668**, 385 (2003).

[129] J. Urheim (CLEO Collaboration), "The hadronic current in tau lepton decay to two pseudoscalar mesons," Nucl.Phys.Proc.Suppl. **55C**, 359 (1997).

[130] G. Aad et al. (ATLAS Collaboration), "Observation of a new particle in the search for the Standard Model Higgs boson with the ATLAS detector at the LHC," Phys.Lett. **B716**, 1 (2012), 1207.7214.

[131] S. Chatrchyan et al. (CMS Collaboration), "Observation of a new boson at a mass of 125 GeV with the CMS experiment at the LHC," Phys.Lett. **B716**, 30 (2012), 1207.7235.

[132] T. Aaltonen et al. (CDF Collaboration), "Evidence for $t\bar{t}\gamma$ Production and Measurement of $\sigma_t\bar{t}\gamma/\sigma_t\bar{t}$," Phys.Rev. **D84**, 031104 (2011), 1106.3970.

[133] C. Collaboration (CMS Collaboration), "Measurement of the inclusive top-quark pair + photon production cross section in the muon + jets channel in pp collisions at 8 TeV," (2014).

[134] 1204229, "Measurement of the inclusive t tbar gamma cross section with the ATLAS detector," (2011).

[135] W. Hollik, "Radiative Corrections in the Standard Model and their Role for Precision Tests of the Electroweak Theory," Fortsch.Phys. **38**, 165 (1990).

[136] J. Bernabeu, J. Vidal, and G. Gonzalez-Sprinberg, "The Weak magnetic moment of heavy quarks," Phys.Lett. **B397**, 255 (1997), hep-ph/9702222.

[137] W. Bernreuther, R. Bonciani, T. Gehrmann, R. Heinesch, T. Leineweber, et al., "Two-loop QCD corrections to the heavy quark form-factors: The Vector contributions," Nucl.Phys. **B706**, 245 (2005), hep-ph/0406046.

[138] W. Bernreuther, R. Bonciani, T. Gehrmann, R. Heinesch, T. Leineweber, et al., "Two-loop QCD corrections to the heavy quark form-factors: Axial vector contributions," Nucl.Phys. **B712**, 229 (2005), hep-ph/0412259.

[139] W. Bernreuther, R. Bonciani, T. Gehrmann, R. Heinesch, T. Leineweber, et al., "Two-loop QCD corrections to the heavy quark form-factors: Anomaly contributions," Nucl.Phys. **B723**, 91 (2005), hep-ph/0504190.

[140] W. Bernreuther, R. Bonciani, T. Gehrmann, R. Heinesch, T. Leineweber, et al., "QCD corrections to static heavy quark form-factors," Phys.Rev.Lett. **95**, 261802 (2005), hep-ph/0509341.

[141] A. Grozin, P. Marquard, J. Piclum, and M. Steinhauser, "Three-Loop Chromomagnetic Interaction in HQET," Nucl.Phys. **B789**, 277 (2008), 0707.1388.

[142] J. Aguilar-Saavedra, "A Minimal set of top anomalous couplings," Nucl.Phys. **B812**, 181 (2009), 0811.3842.

[143] C. Zhang and S. Willenbrock, "Effective-Field-Theory Approach to Top-Quark Production and Decay," Phys.Rev. **D83**, 034006 (2011), 1008.3869.

[144] J. Aguilar-Saavedra, M. Fiolhais, and A. Onofre, "Top Effective Operators at the ILC," JHEP **1207**, 180 (2012), 1206.1033.

[145] B. Grzadkowski, Z. Hioki, K. Ohkuma, and J. Wudka, "Probing anomalous top quark couplings induced by dimension-six operators at photon colliders," Nucl.Phys. **B689**, 108 (2004), hep-ph/0310159.

[146] S. Chatrchyan et al. (CMS Collaboration), "Measurement of the single-top-quark t-channel cross section in pp collisions at $\sqrt{s} = 7$ TeV," JHEP **1212**, 035 (2012), 1209.4533.

[147] G. Aad et al. (ATLAS Collaboration), "Measurement of the t-channel single top-quark production cross section in pp collisions at $\sqrt{s} = 7$ TeV with the ATLAS detector," Phys.Lett. **B717**, 330 (2012), 1205.3130.

[148] T. Hahn, "Generating Feynman diagrams and amplitudes with FeynArts 3," Comput.Phys.Commun. **140**, 418 (2001), hep-ph/0012260.

[149] N. D. Christensen and C. Duhr, "FeynRules - Feynman rules made easy," Comput.Phys.Commun. **180**, 1614 (2009), 0806.4194.

[150] J. Alwall, M. Herquet, F. Maltoni, O. Mattelaer, and T. Stelzer, "MadGraph 5 : Going Beyond," JHEP **1106**, 128 (2011), 1106.0522.

[151] J. Pumplin, D. Stump, J. Huston, H. Lai, P. M. Nadolsky, et al., "New generation of parton distributions with uncertainties from global QCD analysis," JHEP **0207**, 012 (2002), hep-ph/0201195.

[152] J. Bauer, "Prospects for the Observation of Electroweak Top Quark Production with the CMS Experiment," (????).

[153] S. Chatrchyan et al. (CMS Collaboration), "Identification of b-quark jets with the CMS experiment," JINST **8**, P04013 (2013), 1211.4462.

[154] G. Aad et al. (ATLAS Collaboration), "Measurements of $W\gamma$ and $Z\gamma$ production in pp collisions at $\sqrt{s}$= 7 TeV with the ATLAS detector at the LHC," Phys.Rev. **D87**, 112003 (2013), 1302.1283.

[155] G. Aad et al. (ATLAS Collaboration), "Expected Performance of the ATLAS Experiment - Detector, Trigger and Physics," (2009), 0901.0512.

[156] G. Aad et al. (ATLAS Collaboration), "Measurement of isolated-photon pair production in pp collisions at $\sqrt{s} = 7$ TeV with the ATLAS detector," JHEP **1301**, 086 (2013), 1211.1913.